

This is the **accepted version** of the journal article:

Crespo, Isidro; Giménez-Dejoz, Joan; Porté, Sergio; [et al.]. «Design, synthesis, structure-activity relationships and X-ray structural studies of novel 1-oxopyrimido[4,5-c]quinoline-2-acetic acid derivatives as selective and potent inhibitors of human aldose reductase». European Journal of Medicinal Chemistry, Vol. 152 (2018), p. 160-174. DOI 10.1016/j.ejmech.2018.04.015

This version is available at <https://ddd.uab.cat/record/288486>

under the terms of the  **CC BY-NC-ND** license

Design, synthesis, structure-activity relationships and X-ray structural studies of novel 1-oxo-pyrimido[4,5-c]quinoline-2-acetic acid derivatives as selective and potent inhibitors of human aldose reductase

Isidro Crespo,^{†,#} Joan Giménez-Dejoz,[†] Sergio Porté,[†] Alexandra Cousido-Siah,[‡] André Mitschler,[‡] Alberto Podjarny,[‡] Harris Pratsinis,[§] Dimitris Kletsas,[§] Xavier Parés,[†] Francesc X. Ruiz,^{‡, ^,*} Kamel Metwally,^{¶,*} and Jaume Farrés^{†,*}

[†]Department of Biochemistry and Molecular Biology, Universitat Autònoma de Barcelona, E-08193 Bellaterra, Barcelona, Spain

[‡]Department of Integrated Structural Biology, Institut de Génétique et de Biologie Moléculaire et Cellulaire, CNRS, INSERM, UdS, 1 rue Laurent Fries 67404 CEDEX Illkirch, France

[§]Laboratory of Cell Proliferation and Ageing, Institute of Biosciences and Applications, National Centre of Scientific Research "Demokritos", Athens, Greece

[¶]Department of Medicinal Chemistry, Faculty of Pharmacy, Zagazig University, Zagazig, Egypt

Author Information

***Corresponding Authors**

E-mail: fxavier.ruiz@gmail.com, kametwally@hotmail.com, jaume.farres@uab.cat.

Phone: (+34)93 581 3312. Fax: (+34)93 581 1264.

Present Address

[^](F.X.R.) Center for Advanced Biotechnology and Medicine and Department of Chemistry and Chemical Biology, Rutgers University, Piscataway, New Jersey 08854–5627, United States.

[#](I.C.) ALBA Synchrotron, Carrer de la Llum 2-26, 08290 Cerdanyola del Vallès, Barcelona, Spain.

Abstract

Human aldose reductase (AKR1B1, AR) is a key enzyme of the polyol pathway, catalyzing the reduction of glucose to sorbitol at high glucose concentrations, as those found in diabetic condition. Indeed, AKR1B1 overexpression is related to diabetes secondary complications and, in some cases, with cancer. For many years, research has been focused on finding new AKR1B1 inhibitors (ARIs) to overcome these diseases. Despite the efforts, most of the new drug candidates failed because of their poor pharmacokinetic properties and/or unacceptable side effects. Here we report the synthesis of a series of 1-oxo-pyrimido[4,5-*c*]quinoline-2-acetic acid derivatives as novel ARIs. IC₅₀ assays and X-ray crystallographic studies proved that these compounds are promising hits for further drug development, with high potency and selectivity against AKR1B1. Based on the determined X-ray structures with hit-to-lead compounds, we designed and synthesized a second series that yielded lead compound **68** ($K_{i\text{ app}}$ vs. AKR1B1 = 73 nM). These compounds are related to the previously reported 2-aminopyrimido[4,5-*c*]quinolin-1(2*H*)-ones, which exhibit antimitotic activity. Regardless of their similarity, the 2-amino compounds are unable to inhibit AKR1B1 while the 2-acetic acid derivatives are not cytotoxic against fibrosarcoma HT-1080 cells. Thus, the replacement of the amino group by an acetic acid moiety changes their biological activity, improving their potency as ARIs.

Keywords: 1-oxo-pyrimido[4,5-*c*]quinoline-2-acetic acids; AKR1B1; AKR1B10; molecular modeling; X-ray crystallography.

Abbreviations:

AKR, aldo-keto reductase; AKR1B1, aldo-keto reductase family member 1B1; AKR1B10, aldo-keto reductase family member 1B10; AR, aldose reductase; ARI, AKR1B1 inhibitor; DMEM, Dulbecco's minimal essential medium; EIMS, electron ionization mass spectroscopy; TEA, triethylamine.

1. Introduction

Aldo-keto reductases (AKRs) constitute an oxidoreductase superfamily with ubiquitous distribution in living organisms. Most AKRs are NADP(H)-dependent, monomeric cytosolic proteins. Due to a conserved substrate-binding site (only with few changes) and variable external loops, these enzymes can reduce carbonyl groups of a wide variety of compounds, including carbohydrates, steroids, isoflavonoids, lipid peroxidation products, retinoids and prostaglandins[1,2].

Human aldose reductase (AKR1B1, AR) is a potential therapeutic target against secondary complications of diabetes because of its role in the reduction of glucose to sorbitol. Under normoglycemic conditions, due to the high K_m value of AKR1B1 for glucose ($K_m = 76 \text{ mM}$)[3], the importance of this pathway is limited. But under hyperglycemic conditions, the enzyme is active towards the formation of sorbitol, a potent osmotic regulator. The high production of sorbitol along with its oxidation product, fructose, induces cellular osmotic stress, which in turn promotes the expression of AKR1B1. This would further accentuate the oxidative stress linked to the redox imbalance on cofactor regeneration, accounting for secondary diabetes complications[4,5]. Recently, AKR1B1 has also been shown as the mediator of certain oxidative and inflammatory signaling pathways related to other pathologies, such as cardiovascular disorders, sepsis, and cancer[6].

The use of enzyme inhibitors has been proposed as a good therapeutic strategy to treat diseases associated to the action of AKR1B1, and the aforementioned recent findings have renewed the interest for AKR1B1 as a target. Since AKR1B1 and other members of the AKR superfamily, such as AKR1B10 and AKR1B15, have a very similar active-site topology, selective inhibitors are needed to discriminate between them[4,6–10]. Noteworthy, almost all AKR1B1 inhibitors (ARIs) possess a negatively charged group, *e.g.*, the carboxylic acid function of the acetic acid class of inhibitors, or the imide group of hydantoins and their isosteres. This group interacts with the active-site region where the catalytic residues and the positively-charged nicotinamide moiety of the cofactor are located, the so-called anion-binding site[11]. Adjacent to the AKR1B1 active site, an additional subpocket exists that can be opened by induced fit, the specificity

pocket, giving rise to a significantly enlarged active site. This opening is generally driven by a second, usually hydrophobic, ARI moiety[12,13].

A great number of ARIs have been identified in recent years, but very few of them showed sufficient therapeutic efficacy in clinical trials, with epalrestat as the only ARI commercially available to date. Most of the drug candidates failed due to poor pharmacokinetic properties, toxicity and/or unspecific *in vivo* action[14]. Therefore, new ARI scaffolds with an improved profile are needed.

Previously, Metwally and coworkers[15] characterized the 2-aminopyrimido[4,5-*c*]quinolin-1(2*H*)-one scaffold, seeking inhibition of tubulin polymerization. They have expanded the structure-activity relationship (SAR) of this scaffold, finding that it has anticancer potential[16–19]. Although the overall similarity of this scaffold is low when compared to other ARIs (as shown in **Supplementary data, Table S1**), it shares substructures with alrestatin[20] and zenarestat[21], two potent AKR1B1 inhibitors (Figure 1). In fact, several alrestatin derivatives and other isosteric quinolones have been described as good *in vitro* ARIs[22]. Hence, we surmised that replacement of the 2-amino group by a carboxylic acid moiety could make the 2-aminopyrimido[4,5-*c*]quinolin-1(2*H*)-one scaffold amenable for AKR1B1 inhibition. Here, we synthesized and tested *in vitro* 1-oxo-pyrimido[4,5-*c*]quinoline-2-acetic acid derivatives as new ARIs. Our results showed that some of the derivatives are promising hits for AKR1B1 drug development due to their low IC₅₀ values and high selectivity for AKR1B1, when compared to the closest homologue AKR1B10. Structural information revealed that the high potency of the compounds is not dependent on the opening of the AKR1B1 specificity pocket and that they explore previously unoccupied active-site regions. In addition, these compounds showed low or no cytotoxicity against lung fibrosarcoma HT-1080 cells. Therefore, within the series of 1-oxo-pyrimido[4,5-*c*]quinoline-2-acetic acid derivatives, the lead compound **68**, with a low nanomolar K_{i app} value and complying with the Lipinski's rule of five (**Table S2**), is a promising candidate for further drug development.

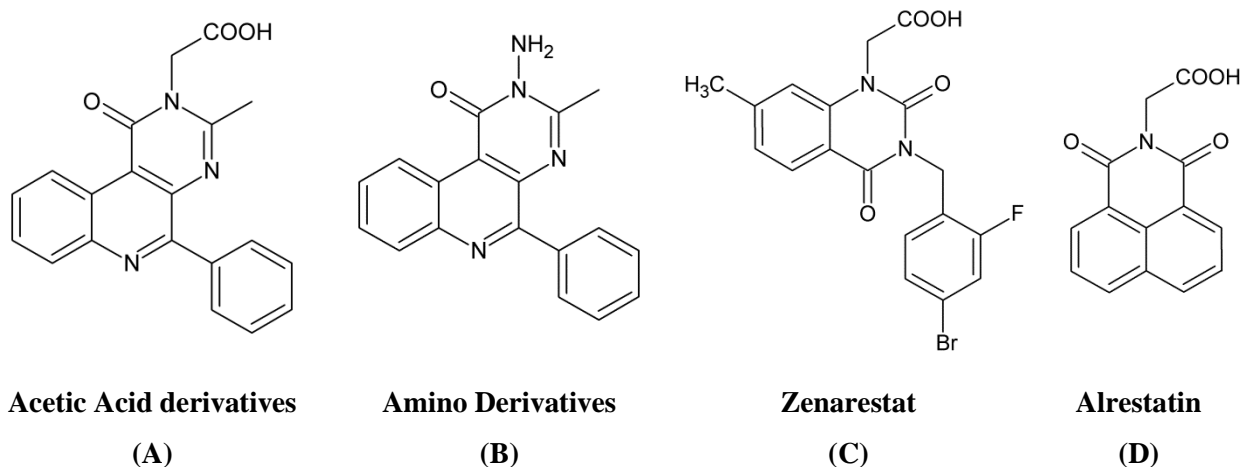


Figure 1. Chemical structures of 1-oxo-pyrimido[4,5-*c*]quinoline-2-acetic acid (A) and 2-aminopyrimido[4,5-*c*]quinolin-1(2*H*)-one (B) derivatives compared to the classical ARIs Zenarestat (C) and Alrestatin (D).

2. Results and discussion

2.1. Design rationale

The initial 2-aminopyrimido[4,5-*c*]quinolin-1(2*H*)-one scaffold (**Figure 1B**) presents a heterocyclic coplanar core reminiscent of alkaloids and flavonoids, with a central quinoline moiety. Indeed, several ARIs obtained from natural sources are related to those two families of metabolites, and some of them exhibit a quinoline moiety[22]. Regarding ARIs, having a quinoline isostere and whose structures in complex with AKR1B1 holoenzyme have been solved by X-ray crystallography, zenarestat and alrestatin are partly superimposable with the initial scaffold (see **Supplementary data**, Similarity Analysis). and both possess a carboxylic acid moiety that interacts with the anion-binding site (**Figure 1**)[20,21] That allowed us to propose the 1-oxo-pyrimido[4,5-*c*]quinoline-2-acetic acid as a putative ARI, given its molecular similarity with the aforementioned ARI[23].

To ascertain the feasibility of our hypothesis, we performed docking analysis of both the initial and the proposed scaffold, including several substitutions based on previous SAR performed with the initial scaffold. Out of the two possible PDB structures amenable to use as docking receptors, we chose the corresponding to the AKR1B1 holoenzyme complexed with zenarestat (PDB ID 1IEI), since the cognate alrestatin complex has two mutations in the active site (PDB ID 1AZ1). **Figure 2** displays the binding modes obtained. In all cases with the 1-oxo-pyrimido[4,5-*c*]quinoline-2-acetic

acid derivatives, the carboxylic acid was located in the anion-binding site, similarly to zenarestat, as we were expecting. Besides, docking was also performed with the other main conformers of AKR1B1 active site[24] and the carboxylic acid of the best poses was also located in the anion-binding site, except in the case of the fidarestat pocket (**Figure S1**). Therefore, we decided to pursue synthesis and SAR of the designed compounds.

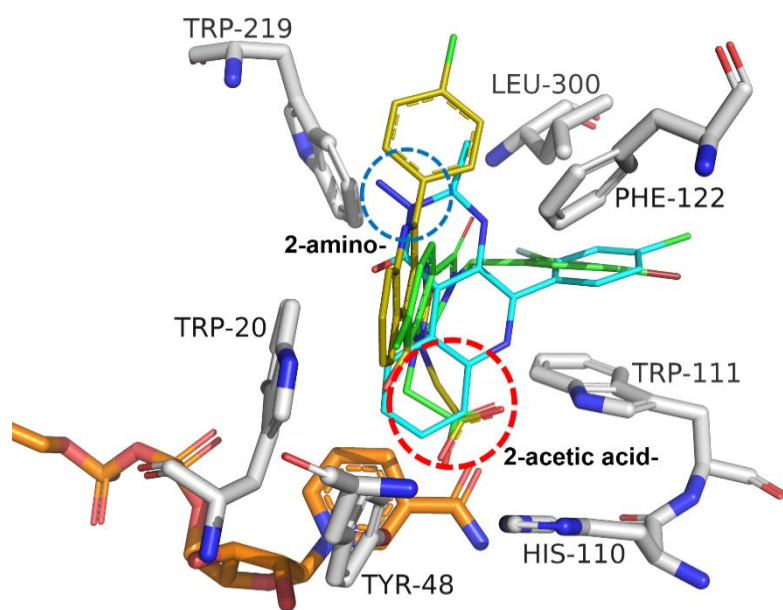


Figure 2. Computed binding mode of **1-oxo-pyrimido[4,5-c]quinoline-2-acetic acid** (gold sticks, 2-acetic acid group circled with red dashes) and **2-aminopyrimido[4,5-c]quinolin-1(2H)-one** (cyan sticks, 2-amino group circled with blue dashes) scaffolds compared to zenarestat (green sticks). The interacting AKR1B1 residues are displayed in white sticks and the NADP⁺ molecule (from PDB ID 1IEI) is displayed in orange sticks.

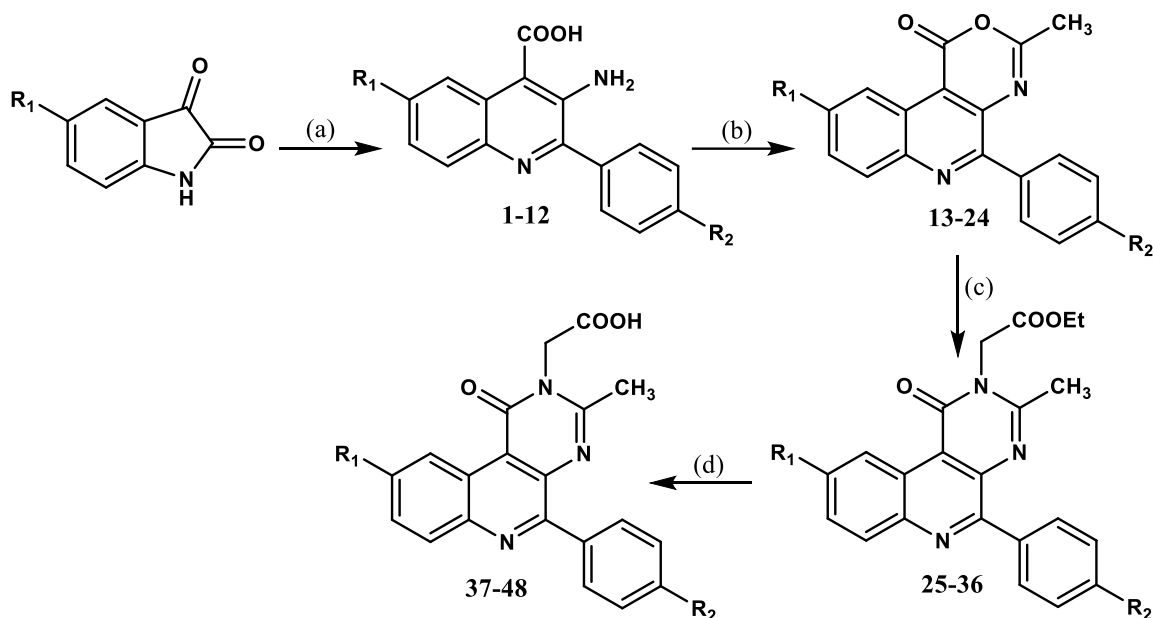
2.2. First series

2.2.1. Chemistry

The first series of target acetic acid derivatives (**37-48**) were synthesized according to the synthetic route outlined in **Scheme 1**. A modified Pfitzinger procedure was adopted to prepare the starting 3-aminoquinoline-4-carboxylic acid derivatives (**1-12**) through reaction of the appropriate isatins with the appropriate phenacylamine hydrochlorides under strongly basic conditions as previously reported[17,25,26].

Cyclization to the desired lactones (**13-24**) was achieved by heating with acetic anhydride. Treatment of the lactones with glycine ethyl ester in the presence of sodium acetate in refluxing acetic acid afforded the acetate esters (**25-36**) in good yields. Basic hydrolysis using aqueous sodium hydroxide gave the desired title compounds (**37-48**) in fair yields.

Scheme 1:



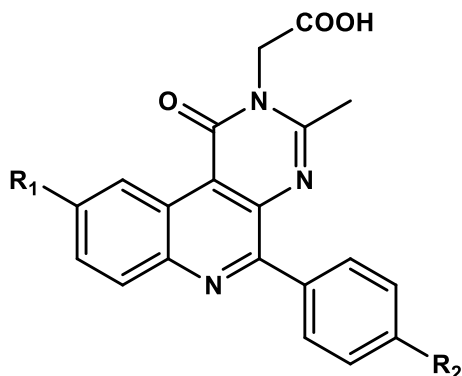
Reagents and conditions:

(a) 4-Substituted phenacylamine hydrochloride, NaOH, EtOH/H₂O/THF, 85 °C to reflux. (b) Acetic anhydride, reflux. (c) Glycine ethyl ester, CH₃COONa, HAc, reflux. (d) Aq. NaOH, 1N, RT.

2.2.2. AKR1B1 and AKR1B10 inhibitor activity

Testing compounds **37** to **48** *in vitro* against AKR1B1 revealed that the most potent inhibitors were compounds **37** to **41** and **44**, displaying IC₅₀ values below 1 μM , while the IC₅₀ values for the other compounds ranged from 1.5 to 5 μM (**Table 1**). AKR1B10 IC₅₀ was included for each compound to establish their relative selectivity for AKR1B1, as shown in **Table 1**. Compounds **37** to **41** and **44**, the most potent for AKR1B1, were also the most selective.

Table 1. Inhibition of AKR1B1 and AKR1B10 by compounds of the first series.



Code	R ₁	R ₂	IC ₅₀ (μM)		AKR1B1 Selectivity
			AKR1B1	AKR1B10	
37	-H	-Cl	0.21 ± 0.04	7.86	37
38	-H	-Br	0.20 ± 0.02	10.00	50
39	-F	-Cl	0.35 ± 0.06	8.18	23
40	-F	-Br	0.57 ± 0.12	9.61	17
41	-F	-OCH ₃	0.26 ± 0.05	10.00	38
42	-Cl	-Cl	1.54 ± 0.12	9.61	6
43	-Cl	-Br	1.92 ± 0.29	13.81	7
44	-Cl	-OCH ₃	0.76 ± 0.09	17.03	22
45	-Br	-Cl	2.22 ± 0.33	17.78	8
46	-Br	-Br	1.57 ± 0.22	16.32	10
47	-CH ₃	-Cl	4.92 ± 0.68	28.46	6
48	-OCH ₃	-Cl	3.14 ± 0.53	15.00	5

2.2.3. *In vitro* cytotoxic activity

Most of the first series derivatives are potent AKR1B1 inhibitors (**Table 1**). To analyze their cytotoxic activity, we tested them against the human fibrosarcoma HT-1080 cell line, using the MTT-assay. The results of 72-h incubation with the test compounds, as well as doxorubicin hydrochloride used as positive control, are shown in **Table 2**. The 2-amino analogues previously described **71** and **72**[15] are also included for comparison (structures are shown in **Table 3**).

Table 2. Cytotoxicity of first series compounds against HT-1080 cells.

Code	Cellular IC ₅₀ (μM)
37	> 100
38	> 100
39	> 100
40	> 100
41	> 100
42	30.2 (± 7.5)
43	> 100
44	78.1 (± 1.1)
45	> 100
46	> 100
47	> 100
48	86.7 (± 3.9)
71	1.23 (± 0.22) [15]
72	1.84 (± 0.40) [15]
Doxorubicin	0.0058 (±0.0029)

The results represent the mean (± standard deviation) of two independent experiments and are expressed as cellular IC₅₀, the concentration that reduced by 50% the optical density of treated cells with respect to untreated controls.

In contrast with the results of the 2-amino compounds **71** and **72**[15], their acidic counterparts displayed no or weak cytotoxic activity, as shown in **Table 2**. Therefore, the substitution of the amino group with an acetic acid moiety substantially decreases cytotoxicity.

2.2.4. X-ray crystallography and structure-activity relationship

X-ray crystallography was used to understand the rationale of the strong inhibition of the 1-oxo-pyrimido[4,5-*c*]quinoline-2-acetic acid scaffold against AKR1B1. Three structures of complexes between AKR1B1 holoenzyme and compounds **37**, **39** and **41** were obtained, at 0.94, 0.96 and 0.96 Å resolution, respectively. **Table S3** shows the data collection and refinement statistics (and **Figure S2** displays $F_o - F_c$ omit maps). All the structures folded into the AKR prototypical (α/β)₈-TIM barrel, with the cofactor position

conserved, and provided a clear understanding of the relevant interactions that make up the AKR1B1-inhibitor complexes.

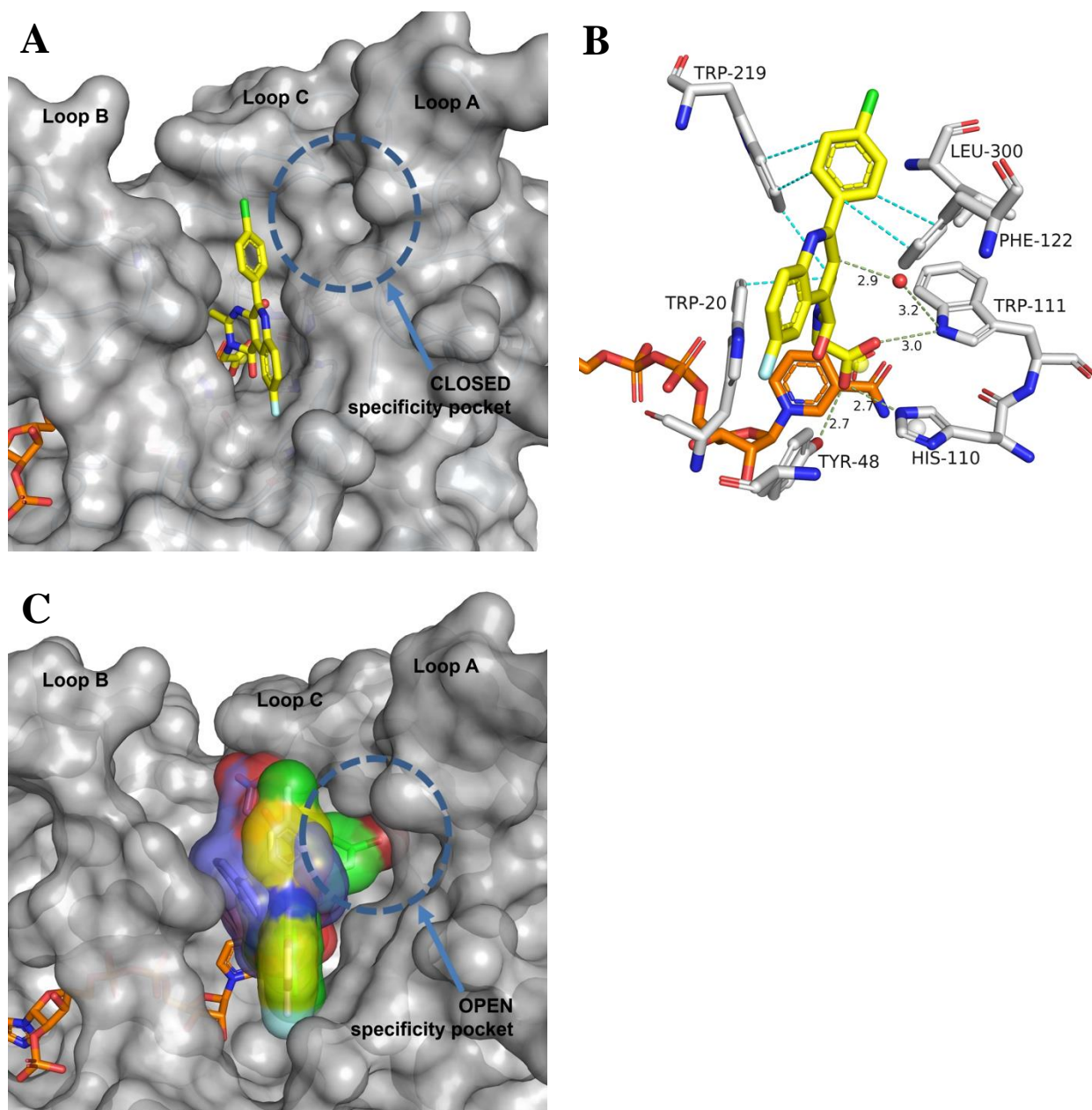


Figure 3. A) Top view of inhibitor **39** (yellow sticks) complexed to AKR1B1 holoenzyme (protein in grey surface and NADP⁺ in orange sticks). B) Atomic representation of the active site of AKR1B1 holoenzyme complexed with **39** (coloring as in A, except for protein residues in white sticks), with distances in Å, hydrogen bonds displayed with smudge green dashed lines and hydrophobic contacts in cyan dashed lines. C) Superimposition of AKR1B1 (surface corresponds to PDB ID 1IEI) complexes with **39** (yellow sticks and surface), alrestatin (violet sticks and surface, two molecules bound in a stacked arrangement) and zenarestat (green sticks and surface).

The inhibitors are oriented in the active site of AKR1B1 laying between loops B and C (**Figures 3A and C**) with the carboxylate head close to the positively charged nicotinamide moiety of the cofactor and forming hydrogen bonds with the OH of Tyr48, the N ϵ 2 of His110, and the N ϵ 1 of Trp111 (**Figure 3B**), in close agreement with our docking predictions (**Figure 2**). Besides, in all the structures there is an interstitial water molecule at 2.9 Å distance from the nitrogen atom of the quinolone ring of the inhibitor (**Figures 3B and S4**). The central pyrimido[4,5-*c*]quinolin-1(2*H*)-one moiety is displaying hydrophobic interactions with Trp20, Phe122 and Trp219, while the 5-phenyl moiety is stacked with Trp219. All these interactions anchor the inhibitor within the enzyme active site (**Figure 2B**).

To note also that, while the acetic acid moiety is located roughly identically in the three structures, the pyrimido[4,5-*c*]quinolin-1(2*H*)-one moiety can relatively swing between Trp20 and Phe122, driven by the distinct interactions of their 5-phenyl moiety (**Figure S3**). Nevertheless, in all three structures, the specificity pocket (localized between Trp111 and Leu300) is not open, remaining in the holoenzyme conformation characterized by a closed loop C (with a closed Leu300, the gatekeeper residue, **Figure 3A**)[4,13].

The inhibition analysis indicates that substituents at the R1 position are the main determinants of the inhibitory potency of this series (**Table 1**). Consistently, the obtained structures show that substituents at the R1 position are important for the inhibitor binding. Thus, R1 groups are located in a solvent exposed region (**Figures 2A and B**). In this sense, compounds **37** to **41**, bearing the smaller and more polar –H or –F at R1, display IC₅₀ values below 1 μM. The rest of the compounds, bearing more apolar substituents (–Cl, –Br, –CH₃ or –OCH₃), display IC₅₀ values above 1 μM (with the exception of **44**). The SAR for the R2 substituents is not that clear-cut. However, the AKR1B1 holoenzyme complex with **41**, which bears a –OCH₃ substituent at R2, is the only one where an R2 group is interacting with the protein (with the main-chain amino groups of Leu301 and Ser302, **Figure S3B**), consistent with a lower IC₅₀ value. Thus, the –OCH₃ substituent in **44** would similarly account for the slightly stronger inhibition of this compound, though other possibilities could not be ruled out. Regarding the AKR1B1 selectivity of the current scaffold over AKR1B10, while no structural information was

obtained with the latter, the most likely explanation might be the differences in loop C residue composition, as loop B is highly conserved in between the two enzymes.

The docking poses obtained were similar to the co-crystallized ligands, but they present some differences (apart from revealing the closed state of the specificity pocket), the most notable being: i) the $-\text{CH}_2-$ of the 2-acetic acid group is flipped in the docking, while in the X-ray structures the whole 2-acetic acid group was superimposable to the cognate group in the AKR1B1-zenarestat complex (**Figure 1**); ii) the R2-substituted aryl moiety is not stacked against Trp219.

We also compared our structures with the previously solved structures of AKR1B1 complexed with alrestatin and zenarestat (PDB IDs 1AZ1 and 1IEI, respectively, **Figure 3C**). Their superimposition allows visualizing that the current compounds and alrestatin bind in a similar manner to the enzyme. On the other hand, zenarestat induces the opening of the specificity pocket (**Figure 3C**). Therefore, we strived to probe the R3 substituent, which appears oriented towards the area where the specificity pocket is located (**Figure 3C**). Interestingly, the parent pyrimido[4,5-*c*]quinolin-1(2*H*)-one scaffold[15] was modified by the addition of a halobenzyl group in R3. Such a moiety is known to open the specificity pocket[27,28]. However, previous studies by us and others[13,29,30] have shown that opening the specificity pocket of AKR1B1 by a compound does not necessarily increase its inhibitory potency. In this regard, we decided to design and synthesize a second series of R3 derivatives contemplating both scenarios, either opening or not the specificity pocket, to assess how this might affect their inhibitory potency.

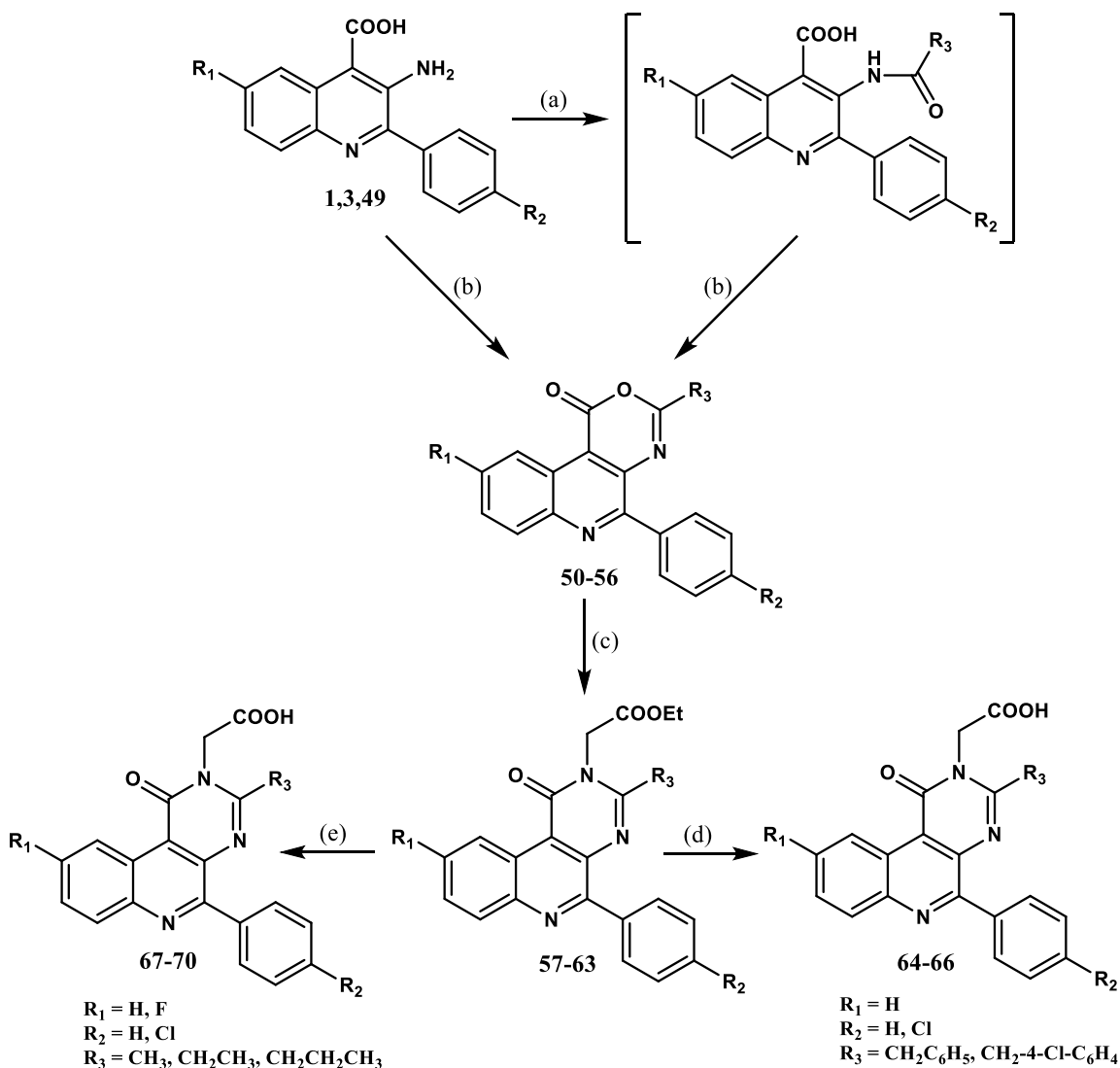
2.3. Second series

2.3.1. Chemistry

The synthetic route was modified in order to obtain the 3-substituted benzyl derivatives of the second series of target compounds (**64-66**) as depicted in **Scheme 2**. Treatment of 3-aminoquinoline-4-carboxylic acid derivatives (**1**, **3**) with phenylacetyl chloride or 4-chlorophenylacetyl chloride in the presence of triethylamine in refluxing THF yielded the N-acyl intermediates which were directly cyclized with acetic anhydride to give the corresponding lactones (**50-52**). The acetate esters (**57-59**) were prepared

following the same procedure used to synthesize their counterparts (**25-36**) as previously mentioned.

Scheme 2:



Reagents and conditions:

(a) Phenylacetyl chloride or 4-chlorophenylacetyl chloride, TEA, THF, reflux. (b) The appropriate acid anhydride, reflux. (c) Glycine ethyl ester, CH_3COONa , HAOc, reflux. (d) HCl/HAOc , Reflux. (e) Aq. NaOH , 1N, RT.

Attempts to hydrolyze the esters using aqueous sodium hydroxide were unsuccessful and gave dark colored reaction mixtures probably due to high reactivity of the benzylic side chain under basic conditions. Finally, the desired target acids (**64-66**)

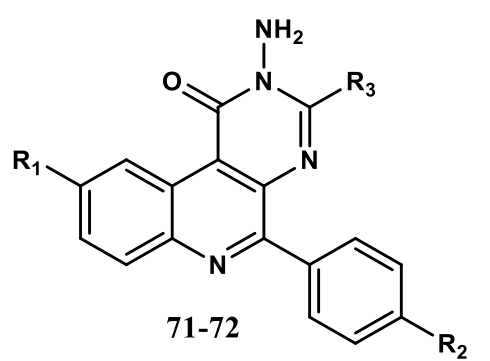
were obtained by hydrolysis of the esters under acidic conditions using a hydrochloric and acetic acid mixture under reflux conditions. The 3-ethyl and 3-propyl substituted acetic acids (**68-70**) were prepared following the same procedure used to prepare their first series analogues with replacing acetic anhydride by propionic and butyric anhydrides, respectively. Compound **67** was obtained in a similar fashion but starting with the unsubstituted 3-aminoquinoline-4-carboxylic acid (**49**). Structures of all the target compounds (**37-48**) and (**64-70**) were characterized by means of mass spectrometry and, ^1H and ^{13}C NMR spectroscopy. Their purity was satisfactorily confirmed by elemental analysis.

2.3.2. *In vitro* AKR1B1 and AKR1B10 inhibitor activity

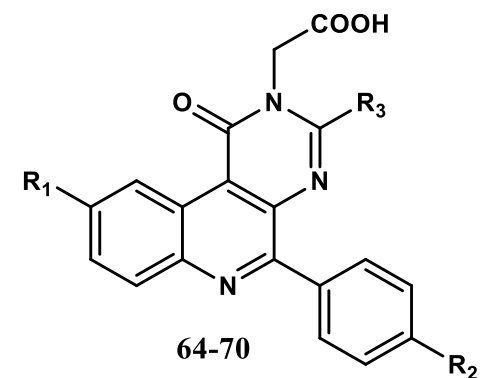
In the second series of compounds, we used **37** as scaffold to probe the R3 substituent, and the inhibitory potency was measured by IC_{50} analysis (**Table 3**). The most potent compounds are **68** and **69**, without an aromatic group in R3. In fact, the most potent compounds of this series, **67-70**, contain an alkyl chain instead. The potency is approximately 10 and 5-fold lower for **65**, with benzyl, than for **68** and **69**, respectively, with an alkyl chain. On the other hand, it can be observed that the addition of fluorine to R1 in **70** decreases the potency by a factor of 4 as compared to **68**, with H in R1. Regarding the selectivity to AKR1B1 in respect to AKR1B10, this second series also seems to improve AKR1B10 inhibitory potency to the point that the selectivity for AKR1B1 is lower. Thus, the SAR behind it will be a subject of further study, given the added difficulty posed by the fact that the active site of AKR1B10 is even more flexible than that of AKR1B1 and presents an extra subpocket at the base of loop A.

We also tested the amino derivatives (compounds **71** and **72**)[15] to determine, by comparison, the effect of the lack of the acidic group. As it can be seen in **Table 3**, no inhibition was observed up to 10 μM level, indicating that despite sharing a structure similar to the 2-amino derivatives, the acetic acid group is essential for AKR1B1 inhibition. This, and the fact that the 2-amino compounds are cytotoxic by tubulin polymerization inhibition[15], make the amino or acidic motif as the selector between the inhibition of tubulin polymerization and AKR1B1.

Table 3. Inhibition of AKR1B1 and AKR1B10 by compounds of the second series.



71-72



64-70

Code	R ₁	R ₂	R ₃	IC ₅₀ (μM)		AKR1B1 Selectivity
				AKR1B1	AKR1B10	
37	-H	-Cl	-CH ₃	0.21± 0.04	7.86	37
64	-H	-Cl	-CH ₂ -C ₆ H ₅	2.65 ± 0.41	2.35	1
65	-H	-Cl	-CH ₂ -4-Cl-C ₆ H ₄	1.01 ± 0.12	2.99	3
66	-H	-H	-CH ₂ -4-Cl-C ₆ H ₄	0.66 ± 0.10	5.87	9
67	-H	-H	-CH ₃	0.43 ± 0.03	6.39	14
68	-H	-Cl	-CH ₂ CH ₃	0.12 ± 0.01	4.71	39
69	-H	-Cl	-CH ₂ CH ₂ CH ₃	0.19 ± 0.03	3.33	18
70	-F	-Cl	-CH ₂ CH ₃	0.41 ± 0.04	3.89	9
71*	-Cl	-Cl	4-Cl-C ₆ H ₄	NI	ND	—
72*	-Cl	-Br	4-Br-C ₆ H ₄	NI	ND	—

NI: No inhibition observed up to 10 μM. ND: Not determined. *Compounds from ref.[15], where the 2-acetic acid group is replaced by a 2-amino group.

The results show that the most potent compounds display IC₅₀ values close to the enzyme concentration used in the assay. It is generally believed that in this case, reversible inhibitors can be considered as tight-binding inhibitors[31]. Adjusting our data to Morrison equation[31] [32], we were able to obtain the value of apparent K_i for the most potent compounds (**Table 4**). Remarkably, the compound **68** showed the lowest apparent K_i value, 73 nM, which ranges within the values for the best ARIs reported[32] and complies with the Lipinski's rule of five (**Table S2**).

Table 4. Apparent K_i values for AKR1B1 using Morrison equation fitting for a tight-binding inhibitor ($IC_{50} < 0.5 \mu M$).

Code	IC_{50} (μM)	$K_{i \text{ app}}$ (μM)
37	0.21 ± 0.04	0.13 ± 0.02
38	0.20 ± 0.02	0.15 ± 0.01
39	0.35 ± 0.06	0.24 ± 0.05
41	0.26 ± 0.05	0.24 ± 0.05
67	0.46 ± 0.03	0.44 ± 0.04
68	0.12 ± 0.004	0.073 ± 0.010
69	0.19 ± 0.03	0.13 ± 0.02
70	0.41 ± 0.04	0.50 ± 0.06

2.3.3. Structure-activity relationship

The SAR studies of the second series of compounds were conducted using the structure of the AKR1B1 holoenzyme complexed to compound **39** as a receptor for molecular docking with Autodock 4. In this complex, the specificity pocket remains in the closed position (**Figures 3A and B**). As expected, the compounds containing an alkyl moiety at R3 could fit well into the receptor, binding in a subpocket at the vicinity of Leu300 (**Figure 4A**), while the compounds bearing an aryl moiety adopted unfavorable poses with the aryl moiety exposed to the solvent (data not shown). The ethyl groups of **68** and **70** exhibit the optimal interaction with Leu300 (**Figure 4B**). As aforementioned, compound **70** displays a 4-fold lower inhibition than **68**. The docking simulations suggest, as a possible reason, that the F atom at R1 might be too close to the carbonyl oxygen of Val47 (**Figure 4C**), which would require an energetically unfavorable rearrangement.

Therefore, the SAR studies of the second series seem to indicate that compounds with a presumably favorable structure for opening the specificity pocket (benzyl group at R3) do not provide interactions that offset the energetic barrier for this process (which is most likely energetically unfavorable[13]), resulting into worse IC_{50} values for AKR1B1. On the other hand, the R3 alkyl compounds can be accommodated in the closed

holoenzyme and provide, in some cases *e.g.* **68** and **69**, additional interactions that slightly increase the inhibitory potency.

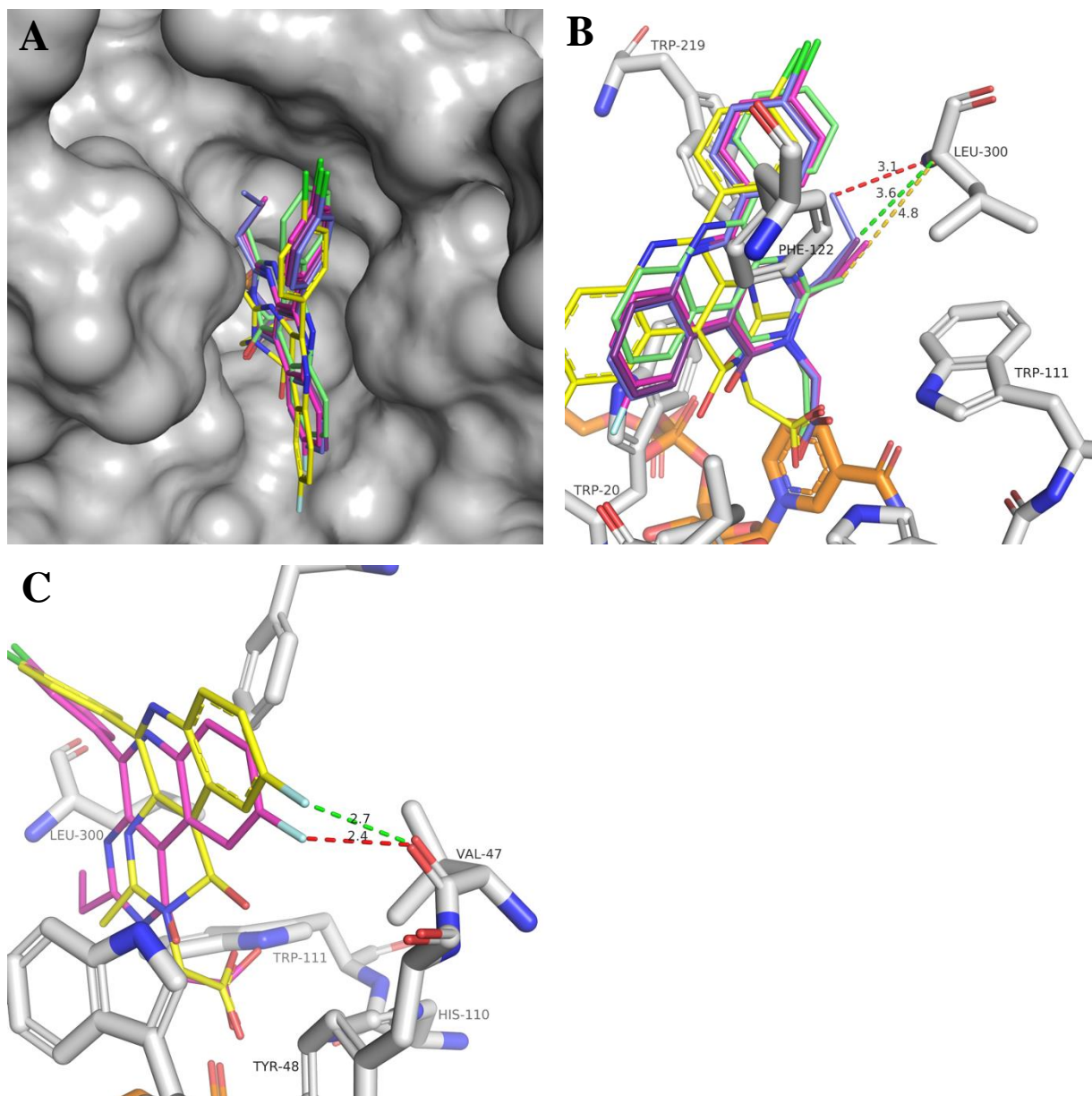


Figure 4. A) Top view of the superimposition of the inhibitor **39** (yellow sticks) complexed to AKR1B1 holoenzyme (protein in grey surface) with the following derivatives of the second series (in sticks): **67** (green), **68** (purple), **69** (purpleblue), **70** (magenta). B) Atomic view of the superimposition displayed in A, including contacts with Leu300 in dashed lines: red (close contact), green (adequate contact), gold (too distant contact). NADP⁺ in orange sticks. C) Atomic view of the superimposition displayed in A, including detail of the F atom contact (**39**: yellow sticks, **70**: magenta sticks) with Val47 of AKR1B1, with distances indicated as in B.

3. Conclusions

In this work, we have been influenced by the structure-based bioisosterism approach to develop novel and pharmacologically-improved ARIs. The term was first utilized by Sheng and coworkers[33] to describe the combination of bioisosterism and molecular modeling in order to design novel triazole antifungal derivatives. As reviewed in ref.[34], bioisosterism is a very useful drug design method to improve pharmacological activity, gain selectivity and optimize the pharmacokinetics of lead compounds. In the current case, however, the replacement of the 2-amino group by the 2-acetic acid has led to achieving a different biological function compared to the original, which is the opposite effect prompted by bioisosterim. To note that we deliberately used the acetic acid moiety for our study, given that this provided a very high likelihood of at least anchoring this novel scaffold to AKR1B1, as proven by experimental and virtual approaches[35].

We initially synthesized the first series of target compounds (**37-48**) with a 3-methyl side chain using acetic anhydride to form the lactones and basic hydrolysis of the intermediate esters to the target acids. This series of compounds have proved to be potent inhibitors of AKR1B1 with appreciable selectivity for it, compared to AKR1B10. Interestingly, they also show low cytotoxicity in cellular experiments. Subsequently, we were interested in improving the AKR1B1 inhibitory profile through a structure-based drug design approach, using both X-ray crystallography and molecular docking. Indeed, these structural studies have provided information that allowed the synthesis of better fitting compounds, and support that their action does not require the opening of the specificity pocket of the enzyme. The structures obtained also show that 1-oxo-pyrimido[4,5-*c*]quinoline-2-acetic acid derivatives occupy a region of the active site, the loop B (featuring Trp219, Figure 3), which previously was only filled by four ARIs out of the 125 deposited in the PDB in complex with AR (csv file and Fig. S5 in Supplementary data).

Next, the synthesis of the second series of target compounds (**64-70**) has probed alkyl as well as benzyl substituents at position 3. In particular, the synthetic route to the 3-benzyl analogues (**64-66**) was modified in order to avoid basic hydrolysis in the final step. From these series, compound **68** has emerged, bearing an alkyl group that

presumably interacts with AKR1B1 having the specificity pocket closed. While the benzyl substituents might open the specificity pocket of AKR1B1, they display worse inhibitory potency than the best compounds of the first series. We hypothesize that this decrease is due to the penalty of opening this pocket without novel interactions strong enough to offset the energetic cost. Supporting our hypothesis, Klebe's group[13] has shown recently in another series of ARIs that there is an energetic barrier (~5 kJ/mol) for opening the specificity pocket of AKR1B1. In conclusion, an important takeaway from this work is that, at least for ARI design, seeking only compounds provoking induced-fit can result in worsening of a series performance. In contrast, a proper space filling of the holoenzyme pocket may be in some instances a better strategy. Investigating the selectivity of the synthesized compounds against AKR1A1 is currently underway.

4. Materials and methods

4.1. Chemistry

4.1.1. General considerations

Melting points are uncorrected and were measured on a Gallenkamp melting point apparatus. ¹H and ¹³C NMR spectra were recorded on Bruker 400-MHz, JEOL RESONANCE 500-MHz, and Varian-Mercury 300-MHz spectrometers. Chemical shifts were expressed in parts per million (ppm) downfield from tetramethylsilane (TMS) and coupling constants (*J*) were reported in Hertz. Mass spectra were recorded on a Shimadzu QP2010 mass spectrometer. Elemental analyses (C, H, and N) were used to determine the purity of all synthesized target compounds, and the results were within ± 0.4% of the calculated values. All compounds were routinely checked by thin-layer chromatography (TLC) on aluminum-backed silica gel plates. All solvents used in this study were dried by standard methods. Intermediate 3-amino-2-(4-substitutedphenyl)-6-substitutedquinoline-4-carboxylic acids (**1-4,6,7,9-12,49**)[17,25,26] and 3-methyl-5-substitutedphenyl-1H-[1,3]oxazino[4,5-c]quinolin-1-ones (**13,14,18**)[15,17] were synthesized following reported procedures.

4.1.2. General procedure for the synthesis of 3-amino-2-(4-substitutedphenyl)-6-substitutedquinoline-4-carboxylic acids (1-12).

A solution of the appropriate phenacylamine hydrochloride (10 mmol) in a mixture of water (18 mL), ethanol (18 mL), and THF (8 mL), was added to a solution of the appropriate isatin (8 mmol) and sodium hydroxide (57 mmol) in water (8 mL) at 85°C, in a dropwise manner over 2 h. The resulting mixture was heated under reflux for additional 30 min. The reaction mixture was concentrated under reduced pressure and filtered through Celite®. The filtrate was acidified with acetic acid and the precipitate obtained was filtered, washed with water, and dried. The crude product was purified by recrystallization from ethanol/ethyl acetate.

4.1.2.1. 2-(4-Methoxyphenyl)-6-fluoro-3-aminoquinoline-4-carboxylic acid (5).

Yield: 51%, mp 224-226 °C; ¹H NMR (DMSO-d₆): δ 3.83 (s, 3H, OCH₃), 7.08-7.11 (m, 2H, Ar-H), 7.24-7.28 (m, 1H, Ar-H), 7.59-7.62 (m, 2H, Ar-H), 7.82-7.87 (m, 1H, Ar-H), 8.16-8.19 (m, 1H, Ar-H). EIMS: *m/z* 312 [M]⁺.

4.1.2.2. 2-(4-Methoxyphenyl)-6-chloro-3-aminoquinoline-4-carboxylic acid (8).

Yield: 54%, mp 242-244 °C; ¹H NMR (DMSO-d₆): δ 3.82 (s, 3H, OCH₃), 7.08-7.10 (m, 2H, Ar-H), 7.36-7.39 (dd, *J*₁ = 2.28, *J*₂ = 8.68 Hz, 1H, Ar-H), 7.60-7.62 (m, 2H, Ar-H), 7.78-7.80 (d, *J* = 8.72 Hz, 1H, Ar-H), 8.48-8.49 (d, *J* = 2.28 Hz, 1H, Ar-H). EIMS: *m/z* 328 [M]⁺.

4.1.3. General procedure for the synthesis of 3,9-disubstituted-5-un/substitutedphenyl-1H-[1,3]oxazino[4,5-c]quinolin-1-ones (13-24, 53-56).

A mixture of the appropriate 3-amino-2-substitutedphenyl-4-quinolinecarboxylic acid (10 mmol) and the appropriate acid anhydride (10 mL) was heated at reflux for 5 h. After cooling, the precipitate was filtered, washed with cold ethanol, and dried. The crude product was recrystallized from either DMF/EtOH or DMF/H₂O.

4.1.3.1. 5-(4-Chlorophenyl)-9-fluoro-3-methyl-1H-[1,3]oxazino[4,5-c]quinolin-1-one (15).

Yield: 67%, mp 218-220 °C (DMF/EtOH); ¹H NMR (DMSO-d₆): δ 2.48 (s, 3H, CH₃), 7.59-7.62 (m, 2H, Ar-H), 7.82-7.87 (m, 1H, Ar-H), 8.01-8.05 (m, 2H, Ar-H), 8.26-8.30

(dd, $J_1 = 7.32$, $J_2 = 9.16$ Hz, 1H, Ar-H), 8.86-8.89 (dd, $J_1 = 2.76$, $J_2 = 11.00$ Hz, 1H, Ar-H). EIMS: m/z 340 $[M]^+$.

4.1.3.2. 5-(4-Bromophenyl)-9-fluoro-3-methyl-1H-[1,3]oxazino[4,5-c]quinolin-1-one (16).

Yield: 67%, mp 204-206 °C (DMF/EtOH); ^1H NMR (DMSO- d_6): δ 2.48 (s, 3H, CH₃), 7.72-7.76 (m, 2H, Ar-H), 7.80-7.85 (m, 1H, Ar-H), 7.93-7.96 (m, 2H, Ar-H), 8.24-8.28 (dd, $J_1 = 5.48$, $J_2 = 9.16$ Hz, 1H, Ar-H), 8.83-8.86 (dd, $J_1 = 2.72$, $J_2 = 11.00$ Hz, 1H, Ar-H). EIMS: m/z 384 $[M]^+$.

4.1.3.3. 5-(4-Methoxyphenyl)-9-fluoro-3-methyl-1H-[1,3]oxazino[4,5-c]quinolin-1-one (17).

Yield: 53%, mp 188-189 °C (DMF/H₂O); ^1H NMR (DMSO- d_6): δ 2.48 (s, 3H, CH₃), 3.84 (s, 3H, OCH₃), 7.07-7.10 (m, 2H, Ar-H), 7.78-7.83 (m, 1H, Ar-H), 7.93-7.96 (m, 1H, Ar-H), 8.02-8.05 (m, 2H, Ar-H), 8.21-8.25 (dd, $J_1 = 5.52$, $J_2 = 9.16$ Hz, 1H, Ar-H), 8.83-8.87 (dd, $J_1 = 3.20$, $J_2 = 11.44$ Hz, 1H, Ar-H). EIMS: m/z 336 $[M]^+$.

4.1.3.4. 5-(4-Bromophenyl)-9-chloro-3-methyl-1H-[1,3]oxazino[4,5-c]quinolin-1-one (19).

Yield: 69%, mp 249-251 °C (DMF/EtOH); ^1H NMR (DMSO- d_6): δ 2.48 (s, 3H, CH₃), 7.74-7.76 (m, 2H, Ar-H), 7.92-7.97 (m, 3H, Ar-H), 8.19-8.22 (d, $J = 9.16$ Hz, 1H, Ar-H), 9.20-9.21 (d, $J = 2.28$ Hz, 1H, Ar-H). EIMS: m/z 402 $[M+2]^+$.

4.1.3.5. 5-(4-Methoxyphenyl)-9-chloro-3-methyl-1H-[1,3]oxazino[4,5-c]quinolin-1-one (20).

Yield: 66%, mp 232-234 °C (DMF/H₂O); ^1H NMR (DMSO- d_6): δ 2.48 (s, 3H, CH₃), 3.85 (s, 3H, OCH₃), 7.08-7.10 (dd, $J_1 = 2.28$, $J_2 = 9.16$ Hz, 1H, Ar-H), 7.89-7.92 (dt, $J = 2.32$, 8.68 Hz, 1H, Ar-H), 8.05-8.07 (dd, $J_1 = 2.28$, $J_2 = 9.08$ Hz, 1H, Ar-H), 8.16-8.18 (dd, $J_1 = 1.84$, $J_2 = 9.16$ Hz, 1H, Ar-H), 9.16-9.20 (t, $J = 1.84$ Hz, 1H, Ar-H). EIMS: m/z 352 $[M]^+$.

4.1.3.6. 5-(4-Chlorophenyl)-9-bromo-3-methyl-1H-[1,3]oxazino[4,5-c]quinolin-1-one (21).

Yield: 63%, mp 241-244 °C (DMF/EtOH); ^1H NMR (DMSO- d_6): δ 2.48 (s, 3H, CH₃), 7.60-7.63 (m, 2H, Ar-H), 8.03-8.15 (m, 4H, Ar-H), 9.37 (s, 1H, Ar-H). EIMS: m/z 402 $[M+2]^+$.

4.1.3.7. 5-(4-Bromophenyl)-9-bromo-3-methyl-1H-[1,3]oxazino[4,5-c]quinolin-1-one (22).

Yield: 70%, mp 238-241 °C (DMF/EtOH); ¹H NMR (DMSO-d₆): δ 2.48 (s, 3H, CH₃), 7.074-7.77 (m, 2H, Ar-H), 7.95-7.98 (m, 2H, Ar-H), 8.03-8.06 (dd, *J*₁ = 2.28, *J*₂ = 9.16 Hz, 1H, Ar-H), 8.12-8.14 (d, *J* = 9.16 Hz, 1H, Ar-H), 9.37-9.38 (d, *J* = 1.84 Hz, 1H, Ar-H). EIMS: *m/z* 446 [M+2]⁺.

4.1.3.8. 5-(4-Chlorophenyl)-3,9-dimethyl-1H-[1,3]oxazino[4,5-c]quinolin-1-one (23).

Yield: 65%, mp 220-222 °C (DMF/EtOH); ¹H NMR (DMSO-d₆): δ 2.36 (s, 3H, CH₃), 2.39 (s, 3H, CH₃), 7.48-7.50 (m, 2H, Ar-H), 7.62-7.65 (dd, *J*₁ = 1.84, *J*₂ = 8.72 Hz, 1H, Ar-H), 7.91-7.98 (m, 3H, Ar-H), 8.89 (s, 1H, Ar-H). EIMS: *m/z* 336 [M]⁺.

4.1.3.9. 5-(4-Chlorophenyl)-9-methoxy-3-methyl-1H-[1,3]oxazino[4,5-c]quinolin-1-one (24).

Yield: 67%, mp 245-246 °C (DMF/EtOH); ¹H NMR (DMSO-d₆): δ 2.46 (s, 3H, CH₃), 3.96 (s, 3H, OCH₃), 7.54-7.60 (m, 3H, Ar-H), 8.01-8.03 (d, *J* = 8.24 Hz, 2H, Ar-H), 8.09-8.12 (d, *J* = 9.40 Hz, 1H, Ar-H), 8.62-8.63 (d, *J* = 2.76 Hz, 1H, Ar-H). EIMS: *m/z* 352 [M]⁺.

4.1.3.10. 5-Phenyl-3-methyl-1H-[1,3]oxazino[4,5-c]quinolin-1-one (53).

Yield: 73%, mp 196-198 °C (DMF/EtOH); ¹H NMR (CDCl₃): δ 2.57 (s, 3H, CH₃), 7.52-7.59 (m, 3H, Ar-H), 7.78-7.88 (m, 2H, Ar-H), 8.07-8.09 (m, 2H, Ar-H), 8.27-8.29 (d, *J* = 8.00 Hz, 1H, Ar-H), 9.35-9.37 (d, *J* = 8.40 Hz, 1H, Ar-H).

4.1.3.11. 5-(4-Chlorophenyl)-3-ethyl-1H-[1,3]oxazino[4,5-c]quinolin-1-one (54).

Yield: 71%, mp 199-200 °C (DMF/EtOH); ¹H NMR (CDCl₃): δ 1.38-1.42 (t, *J* = 7.60 Hz, 3H, CH₃), 2.83-2.88 (q, *J* = 7.60 Hz, 2H, CH₂), 7.52-7.54 (d, *J* = 8.40 Hz, 2H, Ar-H), 7.79-7.88 (tt, *J* = 7.20, 15.60, 31.60 Hz, 2H, Ar-H), 8.12-8.14 (m, 2H, Ar-H), 8.25-8.27 (d, *J* = 8.40 Hz, 1H, Ar-H), 9.35-9.37 (d, *J* = 8.40 Hz, 1H, Ar-H).

4.1.3.12. 5-(4-Chlorophenyl)-3-(1-propyl)-1H-[1,3]oxazino[4,5-c]quinolin-1-one (55).

Yield: 62%, mp 158-160 °C (DMF/H₂O); ¹H NMR (CDCl₃): δ 1.08-1.11 (t, *J* = 7.60 Hz, 3H, CH₃), 1.86-1.96 (m, 2H, CH₂), 2.71-2.81 (t, *J* = 7.60 Hz, 3H, CH₂), 7.52-7.54 (d, *J* = 8.40 Hz, 2H, Ar-H), 7.78-7.88 (m, 2H, Ar-H), 8.10-8.12 (d, *J* = 8.40 Hz, 2H, Ar-H), 8.24-8.26 (d, *J* = 8.00 Hz, 1H, Ar-H), 9.35-9.37 (d, *J* = 8.00 Hz, 1H, Ar-H).

4.1.3.13. 5-(4-Chlorophenyl)-9-fluoro-3-ethyl-1H-[1,3]oxazino[4,5-c]quinolin-1-one (56).

Yield: 64%, mp 185-186 °C (DMF/EtOH); ¹H NMR (CDCl₃): δ 1.39-1.42 (t, *J* = 7.60 Hz, 3H, CH₃), 2.83-2.89 (q, *J* = 7.60 Hz, 2H, CH₂), 7.21-7.26 (m, 2H, Ar-H), 7.57-7.62 (m, 1H, Ar-H), 8.15-8.25 (m, 3H, Ar-H), 8.99-9.02 (dd, *J*₁ = 6.80, *J*₂ = 10.40 Hz, 1H, Ar-H).

4.1.4. General procedure for the synthesis of 3-un/substitutedbenzyl-5-un/substitutedphenyl-1H-[1,3]oxazino[4,5-c]quinolin-1-ones (50-52).

The appropriate phenylacetyl chloride (12 mmol) was added to a stirred mixture of the appropriate 3-aminoquinoline-4-carboxylic acid (10 mmol) and TEA (12 mmol) in THF (10 mL), in a dropwise manner at 0°C. After addition was complete, the mixture was heated at reflux for 8 h. The reaction mixture was evaporated under vacuum and the residue was washed several times with n-hexane. Acetic anhydride was added and the mixture was heated at reflux for 3 h. After cooling to room temperature, precipitate was filtered, washed with n-hexane and dried. The crude product was recrystallized from either DMF/EtOH or DMF/H₂O.

4.1.4.1. 5-(4-Chlorophenyl)-3-benzyl-1H-[1,3]oxazino[4,5-c]quinolin-1-one (50).

Yield: 57%, mp 161-162 °C (DMF/H₂O); ¹H NMR (CDCl₃): δ 4.09 (s, 2H, CH₂), 7.40-7.46 (m, 7H, Ar-H), 7.77-7.87 (tt, *J* = 7.20, 14.80, 31.60 Hz, 2H, Ar-H), 8.02-8.04 (d, *J* = 8.40 Hz, 2H, Ar-H), 8.23-8.25 (d, *J* = 8.00 Hz, 1H, Ar-H), 9.32-9.34 (d, *J* = 8.40 Hz, 1H, Ar-H).

4.1.4.2. 5-(4-Chlorophenyl)-3-(4-chlorobenzyl)-1H-[1,3]oxazino[4,5-c]quinolin-1-one (51).

Yield: 53%, mp 177-179 °C (DMF/EtOH); ¹H NMR (CDCl₃): δ 4.06 (s, 2H, CH₂), 7.33-7.40 (m, 4H, Ar-H), 7.45-7.47 (d, *J* = 8.40 Hz, 2H, Ar-H), 7.78-7.88 (m, 2H, Ar-H), 7.97-7.99 (d, *J* = 8.80 Hz, 2H, Ar-H), 8.23-8.25 (d, *J* = 7.60 Hz, 1H, Ar-H), 9.31-9.33 (d, *J* = 7.60 Hz, 1H, Ar-H).

4.1.4.3. 5-Phenyl-3-(4-chlorobenzyl)-1H-[1,3]oxazino[4,5-c]quinolin-1-one (52).

Yield: 61%, mp 141-142 °C (DMF/EtOH); ¹H NMR (CDCl₃): δ 4.06 (s, 2H, CH₂), 7.37-7.52 (m, 7H, Ar-H), 7.80-7.86 (m, 2H, Ar-H), 8.01 (s, 2H, Ar-H), 8.27-8.29 (d, *J* = 6.40 Hz, 1H, Ar-H), 9.33-9.35 (d, *J* = 7.60 Hz, 1H, Ar-H).

4.1.5. General procedure for the synthesis of ethyl 2-(5-(4-un/substitutedphenyl)-3,9-disubstituted-1-oxopyrimido[4,5-c]quinolin-2(1H)yl)acetates (25-36, 57-63).

A mixture of the appropriate lactone (10 mmol), glycine ethyl ester hydrochloride (11 mmol), and anhydrous sodium acetate (20 mmol) in glacial acetic acid (10 mL), was heated at reflux for 24 h. After cooling, the reaction mixture was poured into ice water and the precipitate was filtered, washed with aqueous sodium bicarbonate then washed with water and ethanol and dried. The crude product was recrystallized from either DMF, DMF/EtOH or DMF/H₂O

4.1.5.1. Ethyl 2-(5-(4-chlorophenyl)-3-methyl-1-oxopyrimido[4,5-c]quinolin-2(1H)yl)acetate (25).

Yield: 62%, mp 212-214 °C (DMF/H₂O); ¹H NMR (DMSO-d₆): δ 1.09-1.13 (t, *J* = 6.88 Hz, 3H, CH₃), 2.37 (s, 3H, CH₃), 4.06-4.11 (q, *J* = 6.88 Hz, 2H, CH₂), 4.93 (s, 2H, CH₂), 7.45-7.49 (m, 2H, Ar-H), 7.68-7.74 (m, 2H, Ar-H), 7.98-8.00 (m, 2H, Ar-H), 8.04-8.07 (m, 1H, Ar-H), 9.43-9.45 (m, 1H, Ar-H). EIMS: *m/z* 407 [M]⁺.

4.1.5.2. Ethyl 2-(5-(4-bromophenyl)-3-methyl-1-oxopyrimido[4,5-c]quinolin-2(1H)yl)acetate (26).

Yield: 64%, mp 216-219 °C (DMF/EtOH); ¹H NMR (DMSO-d₆): δ 1.22-1.25 (t, *J* = 6.88 Hz, 3H, CH₃), 2.60 (s, 3H, CH₃), 4.18-4.22 (q, *J* = 6.88 Hz, 2H, CH₂), 5.04 (s, 2H, CH₂), 7.71-7.73 (d, *J* = 8.24 Hz, 2H, Ar-H), 7.77-7.86 (m, 2H, Ar-H), 8.02-8.04 (m, 2H, Ar-H), 8.15-8.17 (d, *J* = 8.24 Hz, 1H, Ar-H), 9.53-9.55 (d, *J* = 8.24 Hz, 1H, Ar-H). EIMS: *m/z* 453 [M+2]⁺.

4.1.5.3. Ethyl 2-(5-(4-chlorophenyl)-9-fluoro-3-methyl-1-oxopyrimido[4,5-c]quinolin-2(1H)yl)acetate (27).

Yield: 58%, mp 255-257 °C (DMF/EtOH); ¹H NMR (DMSO-d₆): δ 1.09-1.12 (t, *J* = 7.08 Hz, 3H, CH₃), 2.36 (s, 3H, CH₃), 4.07-4.11 (q, *J* = 6.92 Hz, 2H, CH₂), 4.92 (s, 2H, CH₂), 7.45-7.47 (d, *J* = 8.24 Hz, 2H, Ar-H), 7.60-7.65 (ddd, *J*₁ = 3.20, *J*₂ = 8.68, *J*₃ = 17.40 Hz, 1H, Ar-H), 7.95-7.97 (m, 2H, Ar-H), 8.08-8.12 (dd, *J*₁ = 5.96, *J*₂ = 9.20 Hz, 1H, Ar-H), 9.07-9.11 (dd, *J*₁ = 2.72, *J*₂ = 11.44 Hz, 1H, Ar-H). EIMS: *m/z* 425 [M]⁺.

4.1.5.4. Ethyl 2-(5-(4-bromophenyl)-9-fluoro-3-methyl-1-oxopyrimido[4,5-c]quinolin-2(1H)yl)acetate (28).

Yield: 49%, mp 244-247 °C (DMF/EtOH); ¹H NMR (DMSO-d₆): δ 1.09-1.12 (t, *J* = 6.88 Hz, 3H, CH₃), 2.39 (s, 3H, CH₃), 4.05-4.09 (q, *J* = 6.84 Hz, 2H, CH₂), 4.92 (s, 2H, CH₂), 7.59-7.64 (m, 3H, Ar-H), 7.88-7.91 (m, 2H, Ar-H), 8.09-8.13 (dd, *J*₁ = 5.96, *J*₂ = 9.16 Hz, 2H, Ar-H), 9.08-9.12 (dd, *J*₁ = 2.76, *J*₂ = 11.44 Hz, 1H, Ar-H). EIMS: *m/z* 471 [M+2]⁺.

4.1.5.5. *Ethyl 2-(5-(4-methoxyphenyl)-9-fluoro-3-methyl-1-oxopyrimido[4,5-c]quinolin-2(1H)yl)acetate (29)*.

Yield: 50%, mp 215-217 °C (DMF/EtOH); ¹H NMR (DMSO-d₆): δ 1.22-1.26 (t, *J* = 6.88 Hz, 3H, CH₃), 2.62 (s, 3H, CH₃), 3.85 (s, 3H, OCH₃), 4.20-4.24 (q, *J* = 6.88 Hz, 2H, CH₂), 5.05 (s, 2H, CH₂), 7.06-7.09 (m, 2H, Ar-H), 7.71-7.76 (ddd, *J*₁ = 6.40, *J*₂ = 8.24, *J*₃ = 14.20 Hz, 1H, Ar-H), 8.09-8.13 (m, 2H, Ar-H), 8.18-8.22 (dd, *J*₁ = 5.52, *J*₂ = 9.16 Hz, 1H, Ar-H), 9.20-9.24 (dd, *J*₁ = 2.76, *J*₂ = 11.48 Hz, 1H, Ar-H). EIMS: *m/z* 421 [M]⁺.

4.1.5.6. *Ethyl 2-(5-(4-chlorophenyl)-9-chloro-3-methyl-1-oxopyrimido[4,5-c]quinolin-2(1H)yl)acetate (30)*.

Yield: 52%, mp 253-255 °C (DMF/EtOH); ¹H NMR (DMSO-d₆): δ 1.19-1.22 (t, *J* = 6.84 Hz, 3H, CH₃), 2.46 (s, 3H, CH₃), 4.15-4.20 (q, *J* = 6.84 Hz, 2H, CH₂), 5.02 (s, 2H, CH₂), 7.56-7.58 (d, *J* = 8.24 Hz, 2H, Ar-H), 7.84-7.87 (dd, *J*₁ = 6.32, *J*₂ = 8.72 Hz, 1H, Ar-H), 8.07-8.09 (d, *J* = 6.68 Hz, 2H, Ar-H), 8.15-8.17 (d, *J* = 8.72 Hz, 1H, Ar-H), 9.55-9.56 (d, *J* = 2.28, 1H, Ar-H). EIMS: *m/z* 441 [M]⁺.

4.1.5.7. *Ethyl 2-(5-(4-bromophenyl)-9-chloro-3-methyl-1-oxopyrimido[4,5-c]quinolin-2(1H)yl)acetate (31)*.

Yield: 60%, mp 253-256 °C (DMF/EtOH); ¹H NMR (DMSO-d₆): δ 1.22-1.24 (t, *J* = 5.84 Hz, 3H, CH₃), 2.62 (s, 3H, CH₃), 4.18-4.23 (q, *J* = 6.84 Hz, 2H, CH₂), 5.05 (s, 2H, CH₂), 7.72-7.74 (m, 2H, Ar-H), 7.86-7.89 (m, 1H, Ar-H), 8.01-8.04 (m, 2H, Ar-H), 8.16-8.19 (m, 1H, Ar-H), 9.57 (s, 1H, Ar-H). EIMS: *m/z* 487 [M+2]⁺.

4.1.5.8. *Ethyl 2-(5-(4-methoxyphenyl)-9-chloro-3-methyl-1-oxopyrimido[4,5-c]quinolin-2(1H)yl)acetate (32)*.

Yield: 52%, mp 235-237 °C (DMF/H₂O); ¹H NMR (DMSO-d₆): δ 1.22-1.25 (t, *J* = 6.88 Hz, 3H, CH₃), 2.62 (s, 3H, CH₃), 3.84 (s, 3H, OCH₃), 4.18-4.23 (q, *J* = 6.88 Hz, 2H, CH₂), 5.03 (s, 2H, CH₂), 7.06-7.08 (m, 2H, Ar-H), 7.81-7.84 (dd, *J*₁ = 2.28, *J*₂ = 8.72 Hz, 1H, Ar-H), 8.10-8.13 (dd, *J*₁ = 2.28, *J*₂ = 9.16 Hz, 2H, Ar-H), 9.52-9.53 (d, *J* = 2.28, 1H, Ar-H). EIMS: *m/z* 437 [M]⁺.

4.1.5.9. Ethyl 2-(5-(4-chlorophenyl)-9-bromo-3-methyl-1-oxopyrimido[4,5-c]quinolin-2(1H)yl)acetate (**33**).

Yield: 56%, mp 251-253 °C (DMF/EtOH); ¹H NMR (DMSO-d₆): δ 1.22-1.26 (t, *J* = 6.84 Hz, 3H, CH₃), 2.62 (s, 3H, CH₃), 4.18-4.24 (q, *J* = 6.88 Hz, 2H, CH₂), 5.05 (s, 2H, CH₂), 7.58-7.60 (d, *J* = 8.72 Hz, 2H, Ar-H), 7.96-7.97 (dd, *J*₁ = 2.28, *J*₂ = 9.16 Hz, 1H, Ar-H), 8.07-8.11 (m, 3H, Ar-H), 9.72 (s, 1H, Ar-H). EIMS: *m/z* 487 [M+2]⁺.

4.1.5.10. Ethyl 2-(5-(4-bromophenyl)-9-bromo-3-methyl-1-oxopyrimido[4,5-c]quinolin-2(1H)yl)acetate (**34**).

Yield: 57%, mp 256-259 °C (DMF); ¹H NMR (DMSO-d₆): δ 1.22-1.25 (t, *J* = 6.88 Hz, 3H, CH₃), 2.61 (s, 3H, CH₃), 4.18-4.23 (q, *J* = 6.88 Hz, 2H, CH₂), 5.04 (s, 2H, CH₂), 7.72-7.74 (m, 2H, Ar-H), 7.97-78.10 (Complex m, 4H, Ar-H), 9.72-9.74 (m, 1H, Ar-H).

4.1.5.11. Ethyl 2-(5-(4-chlorophenyl)-3,9-dimethyl-1-oxopyrimido[4,5-c]quinolin-2(1H)yl)acetate (**35**).

Yield: 61%, mp 255-257 °C (DMF/EtOH); ¹H NMR (DMSO-d₆): δ 1.12-1.14 (t, *J* = 6.88 Hz, 3H, CH₃), 2.38 (s, 3H, CH₃), 2.46 (s, 3H, CH₃), 4.07-4.12 (q, *J* = 6.88 Hz, 2H, CH₂), 4.92 (s, 2H, CH₂), 7.46-7.48 (m, 2H, Ar-H), 7.56-7.58 (d, *J* = 8.72 Hz, 1H, Ar-H), 7.93-7.99 (m, 3H, Ar-H), 9.25 (s, 1H, Ar-H). EIMS: *m/z* 421 [M]⁺.

4.1.5.12. Ethyl 2-(5-(4-chlorophenyl)-9-methoxy-3-methyl-1-oxopyrimido[4,5-c]quinolin-2(1H)yl)acetate (**36**).

Yield: 59%, mp 246-248 °C (DMF/EtOH); ¹H NMR (DMSO-d₆): δ 1.19-1.22 (t, *J* = 7.32 Hz, 3H, CH₃), 2.56 (s, 3H, CH₃), 3.90 (s, 3H, OCH₃), 4.15-4.20 (q, *J* = 7.32 Hz, 2H, CH₂), 5.01 (s, 2H, CH₂), 7.44-7.47 (dd, *J*₁ = 2.76, *J*₂ = 8.72 Hz, 1H, Ar-H), 7.52-7.54 (m, 2H, Ar-H), 8.04-8.06 (m, 3H, Ar-H), 9.00-9.01 (d, *J* = 2.76, 1H, Ar-H). EIMS: *m/z* 437 [M]⁺.

4.1.5.13. Ethyl 2-(5-(4-chlorophenyl)-3-benzyl-1-oxopyrimido[4,5-c]quinolin-2(1H)yl)acetate (**57**).

Yield: 57%, mp 218-220 °C (DMF/EtOH); ¹H NMR (CDCl₃): δ 1.30-1.34 (t, *J* = 7.20 Hz, 3H, CH₃), 4.22 (s, 2H, CH₂), 4.23-4.29 (q, *J* = 7.20 Hz, 2H, CH₂), 4.95 (s, 2H, CH₂), 7.26-7.29 (m, 3H, Ar-H), 7.35-7.42 (m, 4H, Ar-H), 7.75-7.84 (m, 2H, Ar-H), 8.06-8.08 (d, *J* = 8.80 Hz, 2H, Ar-H), 8.26-8.28 (d, *J* = 7.60 Hz, 1H, Ar-H), 9.67-9.69 (d, *J* = 8.00 Hz, 1H, Ar-H).

4.1.5.14. Ethyl 2-(5-(4-chlorophenyl)-3-(4-chlorobenzyl)-1-oxopyrimido[4,5-c]quinolin-2(1H)yl)acetate (**58**).

Yield: 51%, mp 245-246 °C (DMF/EtOH); ¹H NMR (CDCl₃): δ 1.33-1.36 (t, *J* = 6.40 Hz, 3H, CH₃), 4.16 (s, 2H, CH₂), 4.26-4.32 (q, *J* = 6.40 Hz, 2H, CH₂), 4.96 (s, 2H, CH₂), 7.18-7.20 (m, 2H, Ar-H), 7.35-7.40 (m, 4H, Ar-H), 7.77-7.83 (m, 2H, Ar-H), 7.95-7.98 (d, *J* = 7.60 Hz, 2H, Ar-H), 8.26-8.28 (d, *J* = 7.60 Hz, 1H, Ar-H), 9.66-9.68 (d, *J* = 8.00 Hz, 1H, Ar-H).

4.1.5.15. Ethyl 2-(5-phenyl-3-(4-chlorobenzyl)-1-oxopyrimido[4,5-c]quinolin-2(1H)yl)acetate (**59**).

Yield: 61%, mp 212-214 °C (DMF/EtOH); ¹H NMR (CDCl₃): δ 1.31-1.35 (t, *J* = 6.80 Hz, 3H, CH₃), 4.16 (s, 2H, CH₂), 4.25-4.30 (q, *J* = 6.84 Hz, 2H, CH₂), 4.95 (s, 2H, CH₂), 7.19-7.20 (d, *J* = 7.60 Hz, 2H, Ar-H), 7.32-7.34 (d, *J* = 8.00 Hz, 2H, Ar-H), 7.43-7.45 (d, *J* = 7.20 Hz, 2H, Ar-H), 7.74-7.78 (t, *J* = 7.60 Hz, 1H, Ar-H), 7.81-7.84 (t, *J* = 7.60 Hz, 1H, Ar-H), 7.99-8.00 (d, *J* = 6.80 Hz, 2H, Ar-H), 8.01-8.04 (m, 2H, Ar-H), 8.28-8.30 (d, *J* = 7.60 Hz, 1H, Ar-H).

4.1.5.16. Ethyl 2-(5-phenyl-3-methyl-1-oxopyrimido[4,5-c]quinolin-2(1H)yl)acetate (**60**).

Yield: 55%, mp 236-238 °C (DMF/EtOH); ¹H NMR (CDCl₃): δ 1.34-1.37 (t, *J* = 7.20 Hz, 3H, CH₃), 2.65 (s, 3H, CH₃), 4.30-4.36 (q, *J* = 7.20 Hz, 2H, CH₂), 4.98 (s, 2H, CH₂), 7.50-7.57 (m, 3H, Ar-H), 7.74-7.84 (m, 2H, Ar-H), 8.13-8.15 (d, *J* = 7.20 Hz, 2H, Ar-H), 8.28-8.30 (d, *J* = 8.00 Hz, 1H, Ar-H), 9.68-9.70 (d, *J* = 8.00 Hz, 1H, Ar-H).

4.1.5.17. Ethyl 2-(5-(4-chlorophenyl)-3-ethyl-1-oxopyrimido[4,5-c]quinolin-2(1H)yl)acetate (**61**).

Yield: 58%, mp 214-216 °C (DMF/H₂O); ¹H NMR (CDCl₃): δ 1.36-1.40 (t, *J* = 8.00 Hz, 6H, 2CH₃), 2.81-2.86 (q, *J* = 6.40 Hz, 2H, CH₂), 4.30-4.35 (q, *J* = 6.40 Hz, 2H, CH₂), 4.99 (s, 2H, CH₂), 7.51-7.53 (d, *J* = 7.60 Hz, 2H, Ar-H), 7.76-7.82 (m, 2H, Ar-H), 8.18-8.20 (d, *J* = 7.20 Hz, 2H, Ar-H), 8.25-8.27 (d, *J* = 7.20 Hz, 1H, Ar-H), 9.67-9.69 (d, *J* = 7.20 Hz, 1H, Ar-H).

4.1.5.18. Ethyl 2-(5-(4-chlorophenyl)-3-(1-propyl)-1-oxopyrimido[4,5-c]quinolin-2(1H)yl)acetate (**62**).

Yield: 59%, mp 210-213 °C (DMF/EtOH); ¹H NMR (CDCl₃): δ 1.06-1.10 (t, *J* = 7.20 Hz, 3H, CH₃), 1.34-1.38 (t, *J* = 7.20 Hz, 3H, CH₃), 1.88-1.97 (m, 2H, CH₂), 2.75-2.79 (t, *J* = 7.20 Hz, 2H, CH₂), 4.30-4.36 (q, *J* = 7.20 Hz, 2H, CH₂), 4.99 (s, 2H, CH₂), 7.51-7.53 (d, *J* = 8.40 Hz, 2H, Ar-H), 7.75-7.84 (m, 2H, Ar-H), 8.14-8.16 (d, *J* = 8.40 Hz, 2H, Ar-H), 8.26-8.28 (d, *J* = 78.00 Hz, 1H, Ar-H), 9.68-9.70 (d, *J* = 8.00 Hz, 1H, Ar-H).

4.1.5.19. Ethyl 2-(5-(4-chlorophenyl)-9-fluoro-3-ethyl-1-oxopyrimido[4,5-c]quinolin-2(1H)yl)acetate (63).

Yield: 57%, mp 218-220 °C (DMF/EtOH); ¹H NMR (CDCl₃): δ 1.35-1.42 (m, 6H, 2CH₃), 2.81-2.87 (q, *J* = 6.80 Hz, 2H, CH₂), 4.31-4.36 (q, *J* = 6.40 Hz, 2H, CH₂), 4.99 (s, 2H, CH₂), 7.21-7.25 (t, *J* = 8.00 Hz, 2H, Ar-H), 7.53-7.57 (t, *J* = 6.80 Hz, 1H, Ar-H), 8.22 (s, 3H, Ar-H), 9.35-9.38 (d, *J* = 6.80 Hz, 1H, Ar-H).

4.1.6. General procedure for the synthesis of 2-(5-(4-un/substitutedphenyl)-3,9-disubstituted-1-oxopyrimido[4,5-c]quinolin-2(1H)yl)acetic acids (37-48, 67-70).

The appropriate ester (10 mmol) was suspended in water (10 mL) and THF was added in portions until the entire solid dissolved. Aqueous sodium hydroxide (5%, 10 mL) was added and the reaction mixture was allowed to stir at room temperature for 10 h. The aqueous layer was separated and acidified with acetic acid and the precipitate was filtered, washed with water and dried. The crude product was recrystallized from either DMF/EtOH or DMF/H₂O.

4.1.6.1. 2-(5-(4-Chlorophenyl)-3-methyl-1-oxopyrimido[4,5-c]quinolin-2(1H)yl)acetic acid (37).

Yield: 52%, mp 292-294 °C (DMF/EtOH); ¹H NMR (DMSO-d₆): δ 2.59 (s, 3H, CH₃), 4.96 (s, 2H, CH₂), 7.58-7.59 (d, *J* = 9.00 Hz, 2H, Ar-H), 7.79-7.86 (m, 2H, Ar-H), 8.09-8.14 (d, *J* = 8.50 Hz, 2H, Ar-H), 8.15-8.17 (d, *J* = 8.00 Hz, 1H, Ar-H), 9.56-9.57 (d, *J* = 8.50 Hz, 1H, Ar-H). ¹³C NMR (DMSO-d₆): δ 23.73 (CH₃), 46.59 (CH₂), 118.33, 123.35, 126.01, 128.05 (2C), 129.44, 129.70, 130.14, 133.09 (2C), 134.34, 137.09, 141.01, 144.59, 156.36, 157.50, 161.40, 169.46 (COOH). Anal. calcd for C₂₀H₁₄ClN₃O₃: C, 63.25; H, 3.72; N, 11.06. Found: C, 63.07; H, 3.81; N, 11.31.

4.1.6.2. 2-(5-(4-Bromophenyl)-3-methyl-1-oxopyrimido[4,5-c]quinolin-2(1H)yl)acetic acid (38).

Yield: 47%, mp 298-300 °C (DMF/EtOH); ¹H NMR (DMSO-d₆): δ 2.38 (s, 3H, CH₃), 4.85 (s, 2H, CH₂), 7.60-7.63 (m, 2H, Ar-H), 7.67-7.75 (m, 2H, Ar-H), 7.91-7.93 (m, 2H, Ar-H), 8.04-8.07 (dd, *J*₁ = 1.36, *J*₂ = 8.24 Hz, 1H, Ar-H), 9.45-9.47 (dd, *J*₁ = 1.84, *J*₂ = 8.72 Hz, 1H, Ar-H). ¹³C NMR (DMSO-d₆): δ 23.73 (CH₃), 46.61 (CH₂), 118.35, 123.16, 123.38, 126.02, 129.46, 129.72, 130.15, 131.00 (2C), 133.36 (2C), 137.47, 141.00, 144.60, 156.48, 157.54, 161.41, 169.46 (COOH). EIMS *m/z* 423 [M]⁺. Anal. calcd for C₂₀H₁₄BrN₃O₃: C, 56.62; H, 3.33; N, 9.90. Found: C, 56.51; H, 3.64; N, 9.87.

4.1.6.3. 2-(5-(4-Chlorophenyl)-9-fluoro-3-methyl-1-oxopyrimido[4,5-*c*]quinolin-2(1H)yl)acetic acid (**39**).

Yield: 50%, mp > 300 °C (DMF/EtOH); ¹H NMR (DMSO-d₆): δ 2.60 (s, 3H, CH₃), 4.96 (s, 2H, CH₂), 7.56-7.58 (d, *J* = 8.72 Hz, 2H, Ar-H), 7.69-7.74 (ddd, *J*₁ = 2.80, *J*₂ = 8.72, *J*₃ = 16.96 Hz, 1H, Ar-H), 8.07-8.09 (d, *J* = 8.72 Hz, 2H, Ar-H), 8.16-8.20 (dd, *J*₁ = 5.96, *J*₂ = 89.16 Hz, 1H, Ar-H), 9.17-9.21 (dd, *J*₁ = 3.2, *J*₂ = 11.92 Hz, 1H, Ar-H). ¹³C NMR (DMSO-d₆): δ 23.77 (CH₃), 46.61 (CH₂), 110.00 (d, *J* = 26.0 Hz), 117.87 (d, *J* = 5.0 Hz), 118.86 (d, *J* = 25.0 Hz), 124.33 (d, *J* = 11.0 Hz), 128.05 (2C), 132.71 (d, *J* = 10.0 Hz), 133.03 (2C), 134.41, 136.76, 141.43 (d, *J* = 27.0 Hz), 155.65 (d, *J* = 3.0 Hz), 158.21, 160.75, 161.33, 163.19, 169.33 (COOH). EIMS: *m/z* 397 [M]⁺. Anal. calcd for C₂₀H₁₃ClFN₃O₃: C, 60.39; H, 3.29; N, 10.56. Found: C, 60.01; H, 3.58; N, 10.67.

4.1.6.4. 2-(5-(4-Bromophenyl)-9-fluoro-3-methyl-1-oxopyrimido[4,5-*c*]quinolin-2(1H)yl)acetic acid (**40**).

Yield: 53%, mp 296-299 °C (DMF/EtOH); ¹H NMR (DMSO-d₆): δ 2.38 (s, 3H, CH₃), 4.85 (s, 2H, CH₂), 7.58-7.65 (m, 3H, Ar-H), 7.88-7.91 (m, 2H, Ar-H), 8.08-8.12 (dd, *J*₁ = 5.96, *J*₂ = 8.80 Hz, 1H, Ar-H), 9.09-9.13 (dd, *J*₁ = 3.2, *J*₂ = 14.64 Hz, 1H, Ar-H). ¹³C NMR (DMSO-d₆): δ 23.77 (CH₃), 46.60 (CH₂), 110.01 (d, *J* = 26.0 Hz), 117.88 (d, *J* = 5.0 Hz), 118.88 (d, *J* = 25.0 Hz), 123.24, 124.34 (d, *J* = 11.0 Hz), 130.99 (2C), 132.72 (d, *J* = 10.0 Hz), 133.30 (2C), 137.13, 141.40 (d, *J* = 31.0 Hz), 155.75, 158.22, 160.75, 161.33, 163.20, 169.33 (COOH). EIMS: *m/z* 443 [M+2]⁺. Anal. calcd for C₂₀H₁₃BrFN₃O₃: C, 54.32; H, 2.96; N, 9.50. Found: C, 54.48; H, 3.18; N, 9.19.

4.1.6.5. 2-(5-(4-Methoxyphenyl)-9-fluoro-3-methyl-1-oxopyrimido[4,5-*c*]quinolin-2(1H)yl)acetic acid (**41**).

Yield: 55%, mp 293-295 °C (DMF/H₂O); ¹H NMR (DMSO-d₆): δ 2.37 (s, 3H, CH₃), 3.72 (s, 3H, OCH₃), 4.83 (s, 2H, CH₂), 6.92-6.95 (dd, *J*₁ = 2.32, *J*₂ = 9.16 Hz, 2H, Ar-H), 7.54-7.58 (m, 1H, Ar-H), 7.96-8.02 (m, 3H, Ar-H), 9.03-9.07 (dt, *J*₁ = 2.28, *J*₂ = 11.92 Hz, 1H, Ar-H). ¹³C NMR (DMSO-d₆): δ 23.76 (CH₃), 46.56 (CH₂), 55.69 (OCH₃), 109.99 (d, *J* = 26.0 Hz), 113.46 (2C), 117.82 (d, *J* = 5.0 Hz), 118.66 (d, *J* = 25.0 Hz), 123.90 (d, *J* = 12.0 Hz), 130.42, 132.45 (d, *J* = 10.0 Hz), 132.87 (2C), 141.57 (d, *J* = 29.0 Hz), 156.28 (d, *J* = 3.0 Hz), 157.84, 160.43, 160.53, 161.47, 162.87, 169.39 (COOH). EIMS: *m/z* 393 [M]⁺. Anal. calcd for C₂₁H₁₆FN₃O₄: C, 64.12; H, 4.10; N, 10.68. Found: C, 63.98; 4.35; 10.78.

4.1.6.6. 2-(5-(4-Chlorophenyl)-9-chloro-3-methyl-1-oxopyrimido[4,5-c]quinolin-2(1H)yl)acetic acid (42).

Yield: 51%, mp > 300 °C (DMF/EtOH); ¹H NMR (DMSO-d₆): δ 2.37 (s, 3H, CH₃), 4.85 (s, 2H, CH₂), 7.45-7.47 (d, *J* = 8.24 Hz, 2H, Ar-H), 7.74-7.75 (d, *J* = 2.28 Hz, 1H, Ar-H), 7.97-8.04 (m, 3H, Ar-H), 9.44-9.45 (d, *J* = 2.28, 1H, Ar-H). ¹³C NMR (DMSO-d₆): δ 23.80 (CH₃), 46.71 (CH₂), 117.50, 124.20, 124.85, 128.13 (2C), 130.05, 132.02, 133.11 (2C), 134.18, 134.60, 136.70, 141.58, 143.03, 156.86, 158.38, 161.31, 169.30 (COOH). EIMS: *m/z* 413 [M]⁺. Anal. calcd for C₂₀H₁₃Cl₂N₃O₃: C, 57.99; H, 3.16; N, 10.14. Found: C, 58.21; 3.45, 9.97.

4.1.6.7. 2-(5-(4-Bromophenyl)-9-chloro-3-methyl-1-oxopyrimido[4,5-c]quinolin-2(1H)yl)acetic acid (43).

Yield: 53%, mp 295-297 °C (DMF/EtOH); ¹H NMR (DMSO-d₆): δ 2.37 (s, 3H, CH₃), 4.85 (s, 2H, CH₂), 7.50-7.62 (m, 2H, Ar-H), 7.72-7.74 (m, 1H, Ar-H), 7.89-7.92 (dd, *J*₁ = 2.40, *J*₂ = 8.40 Hz, 2H, Ar-H), 8.01-8.04 (dd, *J*₁ = 2.80, *J*₂ = 9.20 Hz, 1H, Ar-H), 9.93 (s, 1H, Ar-H). ¹³C NMR (DMF-d₇): δ 23.47 (CH₃), 46.80 (CH₂), 119.01, 123.53, 124.10, 126.56, 129.59, 129.89, 130.59, 131.30 (2C), 133.80 (2C), 138.26, 141.67, 145.40, 157.07, 158.10, 162.07, 169.86 (COOH). EIMS: *m/z* 459 [M+2]⁺. Anal. calcd for C₂₀H₁₃BrClFN₃O₃: C, 52.37; H, 2.86; N, 9.16. Found: C, 52.55; H, 3.08; N, 8.94.

4.1.6.8. 2-(5-(4-Methoxyphenyl)-9-chloro-3-methyl-1-oxopyrimido[4,5-c]quinolin-2(1H)yl)acetic acid (44).

Yield: 51%, mp 292-295 °C (DMF/EtOH); ¹H NMR (DMSO-d₆): δ 2.36 (s, 3H, CH₃), 3.72 (s, 3H, OCH₃), 4.83 (s, 2H, CH₂), 6.93-6.95 (m, 2H, Ar-H), 7.68-7.71 (dd, *J*₁ = 2.32,

$J_2 = 8.72$ Hz, 1H, Ar-H), 7.97-8.01 (m, 3H, Ar-H), 9.42-9.43 (d, $J = 2.76$ Hz, 1H, Ar-H). ^{13}C NMR (DMSO- d_6): δ 23.76 (CH₃), 46.61 (CH₂), 55.71 (OCH₃), 113.48 (2C), 117.36, 123.74, 124.80, 129.80, 130.30, 131.73, 132.98 (2C), 133.47, 141.62, 143.11, 157.28, 157.91, 160.67, 161.36, 169.34 (COOH). EIMS: m/z 409 [M]⁺. Anal. calcd for C₂₁H₁₆ClN₃O₄: C, 61.55; H, 3.94; N, 10.25. Found: C, 61.23; H, 4.08; N, 10.28.

4.1.6.9. 2-(5-(4-Chlorophenyl)-9-bromo-3-methyl-1-oxopyrimido[4,5-c]quinolin-2(1H)yl)acetic acid (45**).**

Yield: 49%, mp 279-281 °C (DMF/EtOH); ^1H NMR (DMF- d_7): δ 2.71 (s, 3H, CH₃), 5.13 (s, 2H, CH₂), 7.76-7.77 (d, $J = 8.50$ Hz, 2H, Ar-H), 8.02-8.03 (d, $J = 2.50$ Hz, 1H, Ar-H), 8.13-8.15 (d, $J = 8.50$ Hz, 1H, Ar-H), 8.16-8.18 (d, $J = 9.00$ Hz, 2H, Ar-H), 9.891-9.894 (d, $J = 1.50$ Hz, 1H, Ar-H). ^{13}C NMR (DMF- d_7): δ 23.55 (CH₃), 46.86 (CH₂), 117.96, 123.36, 123.83, 125.23, 128.63, 131.35 (2C), 132.50, 132.98, 133.80 (2C), 137.81, 142.13, 143.95, 157.58, 158.86, 161.89, 169.70 (COOH). EIMS: m/z 459 [M+2]⁺. Anal. calcd for C₂₀H₁₃BrClN₃O₃: C, 52.37; H, 2.86; N, 9.16. Found: C, 52.24; H, 3.05; N, 8.88.

4.1.6.10. 2-(5-(4-Bromophenyl)-9-bromo-3-methyl-1-oxopyrimido[4,5-c]quinolin-2(1H)yl)acetic acid (46**).**

Yield: 52%, mp 296-298 °C (DMF/EtOH); ^1H NMR (DMSO- d_6): δ 2.62 (s, 3H, CH₃), 4.98 (s, 2H, CH₂), 7.73-7.75 (d, $J = 7.60$ Hz, 2H, Ar-H), 7.98-8.11 (m, 4H, Ar-H), 9.77 (s, 1H, Ar-H). ^{13}C NMR (DMSO- d_6): δ 23.79 (CH₃), 46.69 (CH₂), 117.33, 123.06, 123.45, 124.55, 128.03, 131.05 (2C), 132.08, 132.69, 133.36 (2C), 137.06, 141.48, 143.19, 157.02, 158.34, 161.27, 169.29 (COOH). EIMS: m/z 503 [M+2]⁺, 505 [M+4]⁺. Anal. calcd for C₂₀H₁₃Br₂N₃O₃: C, 47.74; H, 2.60; N, 8.35. Found: C, 47.45; H, 2.65; N, 8.20.

4.1.6.11. 2-(5-(4-Chlorophenyl)-3,9-dimethyl-1-oxopyrimido[4,5-c]quinolin-2(1H)yl)acetic acid (47**).**

Yield: 51%, mp 297-299 °C (DMF/EtOH); ^1H NMR (DMF- d_7): δ 2.60 (s, 3H, CH₃), 2.71 (s, 3H, CH₃), 5.12 (s, 2H, CH₂), 7.59-7.61 (d, $J = 8.50$ Hz, 2H, Ar-H), 7.70-7.72 (d, $J = 8.00$ Hz, 2H, Ar-H), 8.08-8.09 (m, 1H, Ar-H), 8.22-8.24 (d, $J = 8.50$ Hz, 2H, Ar-H). ^{13}C NMR (DMSO- d_6): δ 22.31 (CH₃), 23.68 (CH₃), 46.57 (CH₂), 117.91, 123.34, 125.22, 128.00 (2C), 129.87, 131.45, 133.03 (2C), 134.18, 137.22, 139.29, 141.01, 143.19,

155.19, 157.25, 161.44, 169.41 (COOH). EIMS: m/z 393 $[M]^+$. Anal. calcd for $C_{21}H_{16}ClN_3O_3$: C, 64.05; H, 4.10; N, 10.67. Found: C, 64.01; H, 4.06; N, 11.00.

4.1.6.12. 2-(5-(4-Chlorophenyl)-9-methoxy-3-methyl-1-oxopyrimido[4,5-*c*]quinolin-2(1*H*))yl)acetic acid (**48**).

Yield: 54%, mp > 300 °C (DMF/EtOH); 1H NMR (DMSO- d_6): δ 2.59 (s, 3H, CH₃), 3.94 (s, 3H, OCH₃), 4.95 (s, 2H, CH₂), 7.45-7.48 (dd, $J_1 = 2.76$, $J_2 = 9.16$ Hz, 1H, Ar-H), 7.55-7.57 (m, 2H, Ar-H), 8.04-8.10 (m, 3H, Ar-H), 9.03-9.04 (d, $J = 2.76$ Hz, 1H, Ar-H). 1H NMR (DMF- d_7): δ 23.55 (CH₃), 46.79 (OCH₃), 55.68 (CH₂), 113.63 (2C), 118.04, 124.48, 125.38, 130.09, 131.03, 132.16, 133.44 (2C), 134.05, 142.32, 143.91, 157.95, 158.47, 161.39, 162.04, 169.74 (COOH). EIMS: m/z 409 $[M]^+$. Anal. calcd for $C_{21}H_{16}ClN_3O_4$: C, 61.55; H, 3.94; N, 10.25. Found: C, 61.61; H, 4.05; N, 10.18.

4.1.6.13. 2-(5-Phenyl-3-methyl-1-oxopyrimido[4,5-*c*]quinolin-2(1*H*))yl)acetic acid (**67**).

Yield: 56%, mp > 300 °C (DMF/EtOH); 1H NMR (DMSO- d_6): δ 2.60 (s, 3H, CH₃), 4.98 (s, 2H, CH₂), 7.50-7.56 (m, 3H, Ar-H), 7.77-7.86 (m, 2H, Ar-H), 8.05-8.07 (m, 2H, Ar-H), 8.15-8.17 (d, $J = 7.60$ Hz, 1H, Ar-H), 9.56-9.58 (d, $J = 8.00$ Hz, 1H, Ar-H), 13.47 (s, 1H, COOH). ^{13}C NMR (DMSO- d_6): δ 23.47 (CH₃), 46.58 (CH₂), 118.31, 123.26, 126.03, 127.99 (2C), 129.26, 129.29, 129.65, 130.14, 131.27 (2C), 138.44, 141.14, 144.70, 157.37, 157.85, 161.15, 169.50 (COOH). Anal. calcd for $C_{20}H_{15}N_3O_3$: C, 69.56; H, 4.38; N, 12.17. Found: C, 69.98; H, 4.27; N, 12.54.

4.1.6.14. 2-(5-(4-Chlorophenyl)-3-ethyl-1-oxopyrimido[4,5-*c*]quinolin-2(1*H*))yl)acetic acid (**68**).

Yield: 50%, mp 298-300 °C (DMF/EtOH); 1H NMR (DMF- d_7): δ 1.29-1.32 (t, $J = 7.00$ Hz, 3H, CH₃), 2.99-3.04 (q, $J = 7.00$ Hz, 2H, CH₂), 5.12 (s, 2H, CH₂), 7.62-7.64 (d, $J = 9.00$ Hz, 2H, Ar-H), 7.80-7.89 (m, 3H, Ar-H), 8.20-8.22 (d, $J = 8.00$ Hz, 2H, Ar-H), 8.30-8.31 (d, $J = 8.50$ Hz, 1H, Ar-H). ^{13}C NMR (DMSO- d_6): δ 10.55 (CH₃), 28.03 (CH₂), 45.66 (CH₂), 118.26, 123.38, 126.11, 127.92 (2C), 129.43, 129.72, 130.18, 133.24 (2C), 134.40, 136.94, 140.78, 144.70, 156.35, 160.22, 161.48, 169.52 (COOH). Anal. calcd for $C_{21}H_{16}ClN_3O_3$: C, 64.05; H, 4.10; N, 10.67. Found: C, 63.89; H, 3.85; N, 10.70.

4.1.6.15. 2-(5-(4-Chlorophenyl)-3-(1-propyl)-1-oxopyrimido[4,5-*c*]quinolin-2(1*H*))yl)acetic acid (**69**).

Yield: 55%, mp > 300 °C (DMF/EtOH); ¹H NMR (DMSO-d₆): δ 0.97-1.01 (t, *J* = 7.20 Hz, 3H, CH₃), 1.73-1.82 (m, 2H, CH₂), 2.82-2.86 (q, *J* = 7.20 Hz, 2H, CH₂), 4.96 (s, 2H, CH₂), 7.57-7.59 (d, *J* = 8.40 Hz, 2H, Ar-H), 7.76-7.85 (m, 2H, Ar-H), 8.13-8.15 (d, *J* = 8.40 Hz, 3H, Ar-H), 9.54-9.56 (d, *J* = 8.00 Hz, 1H, Ar-H), 13.43 (s, 1H, COOH). ¹³C NMR (DMSO-d₆): δ 13.97 (CH₃), 19.08 (CH₂), 66.33 (CH₂), 45.81 (CH₂), 118.27, 123.37, 126.10, 127.91 (2C), 129.42, 129.69, 130.16, 133.14 (2C), 134.36, 136.99, 140.79, 144.66, 156.41, 159.36, 161.52, 169.51 (COOH). Anal. calcd for C₂₂H₁₈ClN₃O₃: C, 64.79; H, 4.45; N, 10.30. Found: C, 64.64; H, 4.25; N, 10.42.

4.1.6.16. 2-(5-(4-Chlorophenyl)-9-fluoro-3-ethyl-1-oxopyrimido[4,5-c]quinolin-2(1H)yl)acetic acid (70).

Yield: 52%, mp > 300 °C (DMF/EtOH); ¹H NMR (DMF-d₇): δ 1.30-1.32 (t, *J* = 7.50 Hz, 3H, CH₃), 3.01-3.05 (q, *J* = 7.50 Hz, 2H, CH₂), 5.12 (s, 2H, CH₂), 7.62-7.64 (d, *J* = 8.50 Hz, 2H, Ar-H), 7.76-7.79 (m, 2H, Ar-H), 8.27-8.31 (m, 2H, Ar-H), 9.34-9.37 (dd, *J*₁ = 2.00 Hz, *J*₂ = 11.50 Hz, 1H, Ar-H). ¹³C NMR (DMF-d₇): δ 10.43 (CH₂CH₃), 28.58 (CH₂CH₃), 45.86 (NCH₂), 110.58 (d, *J* = 26.0 Hz), 118.51, 119.05 (d, *J* = 25.0 Hz), 125.10 (d, *J* = 11.9 Hz), 128.23 (2C), 133.20 (d, *J* = 9.6 Hz), 133.62 (2C), 135.09, 137.41, 141.86, 142.57, 156.33, 161.47, 162.07, 163.67, 169.80 (COOH). Anal. calcd for C₂₁H₁₅ClFN₃O₃: C, 61.25; H, 3.67; N, 10.20. Found: C, 61.36; H, 3.45; N, 10.52.

4.1.7. General procedure for the synthesis of 2-(5-(4-un/substitutedphenyl)-3-un/substitutedbenzyl-1-oxopyrimido[4,5-c]quinolin-2(1H)yl)acetic acids (64-66).

A mixture of the appropriate ester (**57-59**; 10 mmol), glacial acetic acid (15 mL) and hydrochloric acid (5 mL) was heated at reflux for 3 h. The reaction mixture was evaporated under reduced pressure and the residue was treated with glacial acetic acid (15 mL) and hydrochloric acid (5 mL) and the mixture was heated at reflux again for 3 h. After cooling to room temperature, the reaction mixture was poured into ice water and the precipitate was filtered, washed with water and ethanol and dried. The crude product was recrystallized from DMF/EtOH.

4.1.7.1. 2-(5-(4-Chlorophenyl)-3-benzyl-1-oxopyrimido[4,5-c]quinolin-2(1H)yl)acetic acid (64):

Yield: 47%, mp 281-283 °C; ¹H NMR (DMF-d₇): δ 4.44 (s, 2H, CH₂), 5.17 (s, 2H, CH₂), 7.40 (s, 5H, Ar-H), 7.82-7.88 (m, 4H, Ar-H), 8.12-8.13 (d, *J* = 7.50 Hz, 2H, Ar-H), 8.20-8.21 (d, *J* = 7.50 Hz, 1H, Ar-H), 9.67-9.69 (d, *J* = 8.00 Hz, 1H, Ar-H). ¹³C NMR (DMF-d₇): δ 41.66 (CH₂), 46.39 (CH₂), 119.07, 123.96, 126.65, 127.57, 128.14 (2C), 129.26 (2C), 129.61, 130.01, 130.51 (2C), 130.58, 133.48 (2C), 134.80, 136.18, 137.30, 141.44, 145.49, 156.23, 159.28, 162.22, 169.65 (COOH). Anal. calcd for C₂₆H₁₈ClN₃O₃: C, 68.50; H, 3.98; N, 9.22. Found: C, 68.32; H, 3.83; N, 9.10.

4.1.7.2. 2-(5-(4-Chlorophenyl)-3-(4-chlorobenzyl)-1-oxopyrimido[4,5-*c*]quinolin-2(1H)yl)acetic acid (**65**).

Yield: 49%, mp 280-282 °C; ¹H NMR (DMF-d₇): δ 4.46 (s, 3H, CH₃), 5.21 (s, 2H, CH₂), 7.37-7.46 (m, 4H, Ar-H), 7.81-7.90 (m, 3H, Ar-H), 8.01-8.04 (m, 3H, Ar-H), 8.19-8.20 (d, *J* = 8.00 Hz, 1H, Ar-H), 9.66-9.68 (d, *J* = 8.00 Hz, 1H, Ar-H). ¹³C NMR (DMF-d₇): δ 40.75 (CH₂), 46.32 (CH₂), 119.02, 123.95, 126.97, 128.06 (2C), 129.19 (2C), 129.64, 130.05, 130.61, 132.67 (2C), 132.76, 133.39 (2C), 134.83, 135.29, 137.22, 141.32, 145.54, 156.27, 159.19, 162.17, 169.72 (COOH). Anal. calcd for C₂₆H₁₇Cl₂N₃O₃: C, 63.69; H, 3.49; N, 8.57. Found: C, 63.42; H, 3.20; N, 8.48.

4.1.7.3. 2-(5-Phenyl-3-(4-chlorobenzyl)-1-oxopyrimido[4,5-*c*]quinolin-2(1H)yl)acetic acid (**66**):

Yield: 45%, mp 271-273 °C; ¹H NMR (DMSO-d₆): δ 4.32 (s, 3H, CH₃), 5.06 (s, 2H, CH₂), 7.30-7.33 (m, 4H, Ar-H), 7.39-7.44 (m, 3H, Ar-H), 7.78-7.91 (m, 4H, Ar-H), 8.16-8.18 (d, *J* = 8.00 Hz, 1H, Ar-H), 8.58-8.61 (d, *J* = 8.40 Hz, 1H, Ar-H), 13.37 (s, 1H, COOH). ¹³C NMR (DMF-d₇): δ 40.81 (CH₂), 46.37 (CH₂), 119.01, 123.85, 126.68, 127.97, 129.18, 129.28, 129.42, 129.96, 130.58, 131.72, 132.50, 132.71, 135.26, 138.58, 141.46, 145.66, 157.75, 158.90, 162.28, 169.72 (COOH). Anal. calcd for C₂₆H₁₈ClN₃O₃: C, 68.50; H, 3.98; N, 9.22. Found: C, 68.73; H, 3.70; N, 8.95.

4.2. Crystallization and structure determination

Co-crystals of AKR1B1–NADP⁺- compounds **37**, **39** and **41** were obtained in 50 mM MES, pH 5.5, 20 mM ammonium sulfate, 20% PEG 6000 by the hanging-drop vapor-diffusion method at 24°C, as reported[4]. Cryo-cooling in liquid nitrogen was carried out using a cryo-protecting solution containing 40% PEG 6000. Data collection

was performed to indicate resolutions at synchrotron Swiss Light Source on the X06DA beamline. The crystals belonged to space group *P1*, with one protein molecule in the asymmetric unit. Data were processed with *HKL-2000*[36]. Data-collection statistics are listed in **Table S3**.

4.3. Structure refinement

The atomic coordinates of the human AKR1B1–NADP⁺–JF0064 complex (PDB ID 4IGS) were used to solve the structures of the above AKR1B1 ternary complexes. Molecular replacement was performed with Phaser[37]. Crystallographic refinement involved repeated cycles of conjugate-gradient energy minimization and temperature-factor refinement performed with *REFMAC5*[38] and *PHENIX*[39]. The ligand PDB files and related restraint dictionaries were built using eLBOW[40]. Amino-acid side chains and water molecules were fitted into $2F_o - F_c$ and $F_o - F_c$ electron-density maps with *Coot*[41]. The final $F_o - F_c$ maps indicated clear electron density for the inhibitor in the three complexes (**Figure S2**). Refinement statistics are presented in **Table S3**. The atomic coordinates have been deposited in the PDB (PDB IDs 5OU0, 5OUJ, 5OUK) and will be released immediately upon publication.

4.4. Docking simulations

To estimate the inhibition constant values of different compounds and their predicted position in the active site of the enzyme, we used Autodock 4.2[42]. The receptor molecule was either one of the following holoenzyme complexes: AKR1B1-zenarestat (PDB ID 1IEI), AKR1B1-tolrestat (PDB ID 2FZD), AKR1B1-fidarestat (PDB ID 1PWM) or AKR1B1-**39** (PDB ID: 5OUJ). All compounds were drawn with ACD/ChemSketch 2016.2 and then were energy-minimized with PRODRG server[43] before starting docking simulations. The PDB files of the receptor and ligands were processed with Autodock tools[42] to add polar hydrogens, compute Gasteiger charges and rename atoms in the Autodock 4.2 format. Gasteiger charges of NADP⁺ molecule on the receptor were manually corrected adding 0.22 eV and 0.37 eV to carbons 2 and 6, respectively[44]. Then, the ligand bonds were allowed to rotate freely.

In all cases, the dimensions of the grid were 50, 40, 40 grid points (x, y, z) (0.375 Å/point). The grid was centered at coordinates: -2.777, -8.072, 10.443 for 5OUJ; -1.015, -0.763, 9.606 for 1IEI; 14.389, -3.838, 14.455 for 1PWM; and 14.312, -3.765, 14.694 for 2FZD. One hundred fifty runs of the genetic algorithm were used as the default option. Results shown correspond to the cluster that includes the highest number of conformations, based on a clusterization of compounds by a RMSD value of 2 Å. Figures were prepared using the Pymol software (DeLano Scientific).

4.5. Inhibition of AKR1B1 and AKR1B10 activity

All determinations were carried out in a Varian Cary 400 (UV/Vis) spectrophotometer. The reaction was followed by the decrease in the absorbance at 340 nm, corresponding to the oxidation of NADPH, using DL-glyceraldehyde as a substrate. Enzymatic inhibition assays were performed in a final reaction volume of 600 µL, containing 0.1 M sodium phosphate, pH 7.5, 0.2 mM NADPH (Apollo Scientific), 1% (v/v) DMSO (Sigma), 100 nM recombinant protein, substrate and the test compound, at 25°C. After adding all compounds except for the substrate, the mixture was incubated for 5 min at room temperature and the reaction was initiated by adding the substrate. Recombinant AKR1B1 and AKR1B10 were obtained as previously described[45]. All compounds were dissolved in DMSO. The concentration of substrate (DL-glyceraldehyde) was 6 and 60 mM for AKR1B1 and AKR1B10, respectively. Percentage of remaining activity was calculated as the activity at a given inhibitor concentration normalized by the control activity with 1% (v/v) DMSO without compound. Results were calculated using GraFit version 5 (Erithacus Software) and are shown as the IC₅₀ value ± standard deviation. To estimate selectivity for AKR1B1, a triplicate at 10 µM concentration was tested with AKR1B10 and the IC₅₀ was computed[46]. The K_{i app} value of compounds with IC₅₀ ≤ 0.5 µM was determined by fitting data to the Morrison equation for tight-binding inhibitors [47]:

$$\frac{v_i}{v_0} = 1 - \frac{([E] + [I] + K_i^{app}) - \sqrt{([E] + [I] + K_i^{app})^2 - 4[E][I]}}{2[E]}$$

The term v_i/v_0 is referred to as the fractional activity remaining at a given inhibitor concentration.

4.6. In vitro cytotoxicity

The compounds were tested for their cytotoxic activity on the human lung fibrosarcoma HT-1080 (American Type Culture Collection, Rockville, MD). Cells were routinely cultured in Dulbecco's minimal essential medium (DMEM; Gibco BRL, Paisley, U.K.) supplemented with penicillin (100 U/mL), streptomycin (100 mg/mL), and 10% fetal bovine serum (media and antibiotics from Biochrom KG, Berlin, Germany) in an environment of 5% CO₂, 85% humidity, and 37 °C, and they were subcultured using a 0.25% trypsin - 0.02% EDTA solution. The cytotoxicity assay was performed by a modification of the MTT method[48,49]. Briefly, the cells were plated at a density of approximately 5000 cells/well in 96-well flat-bottomed microplates, and after 24 h the test compounds were added, diluted in DMSO. After a 72-h incubation, the medium was replaced with MTT (Sigma) dissolved at a final concentration of 1 mg/mL in serum-free, phenol-red-free DMEM for a further 4 h incubation. Then, the MTT formazan was solubilized in 2-propanol and the optical density was measured with a microplate reader at a wavelength of 550 nm (reference wavelength 690 nm). Doxorubicin hydrochloride was included in the experiments as positive control. The results represent the mean of three independent experiments and are expressed as cellular IC₅₀, *i.e.*, the concentration that reduced by 50% the optical density of treated cells with respect to untreated controls.

Author Contributions

The manuscript was written through contributions of all authors.

Conflicts of interest

The authors have no competing financial interests to declare.

Acknowledgements

This work has been funded by the Spanish Ministerio de Economía y Competitividad (BFU2011-24176 and BIO2016-78057). X. Parés and J. Farrés belong to

a research group supported by the Generalitat de Catalunya (2017 SGR 1584). Partial financial support by the Faculty of Pharmacy, Zagazig University (Egypt), by the CNRS, the INSERM, the Université de Strasbourg, the Région Alsace, the Hôpital Civil de Strasbourg, Instruct (part of the European Strategy Forum of Research Infrastructures; ESFRI) and the French Infrastructure for Integrated Structural Biology (FRISBI) ANR-10-INSB-05-01, and by the project “An Open-Access Research Infrastructure of Chemical Biology and Target-Based Screening Technologies for Human and Animal Health, Agriculture and the Environment (OPENSREEN-GR)” (MIS 5002691), which is implemented under the Action “Reinforcement of the Research and Innovation Infrastructure”, funded by the Operational Programme "Competitiveness, Entrepreneurship and Innovation" (NSRF 2014-2020) and co-financed by Greece and the European Union (European Regional Development Fund).

We thank IGBMC Structural Genomics Platform staff in particular Dr. Alastair McEwen and Pierre Poussin-Courmontagne. The crystallographic experiments were performed on the X06DA beamline at the Swiss Light Source synchrotron, Paul Scherrer Institut, Villigen, Switzerland. We thank in particular Vincent Olieric and Takashi Tomizaki for their help in data collection.

Appendix A. Supplementary data

Tables S1-S3 including Tanimoto similarity analysis, calculations for the Lipinski's rule of five, and X-ray crystallography data collection and refinement statistics. Additional **Figures S1-S5** illustrating *F_o-F_c* omit maps and some atomic representations of the active site of AKR1B1 holoenzyme complexed with various compounds. NMR and mass spectra of intermediates and target compounds plus microanalytical results of all final compounds. Output from structure analysis using SIENA (csv file).

References:

- [1] Y. Jin, T. M Penning, Aldo-keto reductases and bioactivation/detoxication, Annu. Rev. Pharmacol. Toxicol. 47 (2007) 263–292.

- [2] Y. Shen, L. Zhong, S. Johnson, D. Cao, Human aldo-keto reductases 1B1 and 1B10: a comparative study on their enzyme activity toward electrophilic carbonyl compounds, *Chem. Biol. Interact.* 191 (2011) 192–198.
- [3] B. Crosas, D. J. Hyndman, O. Gallego, S. Martras, X. Parés, T. G. Flynn, J. Farrés, Human aldose reductase and human small intestine aldose reductase are efficient retinal reductases: consequences for retinoid metabolism, *Biochem. J.* 373 (2003) 973–979.
- [4] A. Cousido-Siah, F. X. Ruiz, A. Mitschler, S. Porté, Á. R. de Lera, M. J. Martín, S. Manzanaro, J. A de la Fuente, F. Terwesten, M. Betz, G. Klebe, J. Farrés, X. Parés, A. Podjarny, Identification of a novel polyfluorinated compound as a lead to inhibit the human enzymes aldose reductase and AKR1B10: structure determination of both ternary complexes and implications for drug design, *Acta Crystallogr. D. Biol. Crystallogr.* 70 (2014) 889–903.
- [5] R. Tammali, S. K. Srivastava, K. V. Ramana, Targeting aldose reductase for the treatment of cancer, *Curr. Cancer Drug Targets* 11 (2011) 560–571.
- [6] R. Maccari, R. Ottanà, Targeting aldose reductase for the treatment of diabetes complications and inflammatory diseases: new insights and future directions. *J. Med. Chem.* 58 (2015) 2047–2067.
- [7] A. Cousido-Siah, F. X. Ruiz, I. Crespo, S. Porté, A. Mitschler, X. Parés, A. Podjarny, J. Farrés, Structural analysis of sulindac as an inhibitor of aldose reductase and AKR1B10. *Chem. Biol. Interact.* 234 (2015) 290–296.
- [8] J. Giménez-Dejoz, M. H. Kolář, F. X. Ruiz, I. Crespo, A. Cousido-Siah, A. Podjarny, O. A. Barski, J. Fanfrlík, X. Parés, J. Farrés, S. Porté, Substrate specificity, inhibitor selectivity and structure-function relationships of aldo-keto reductase 1B15: a novel human retinaldehyde reductase, *PLoS One* 10 (2015) 1–19.
- [9] S. Porté, F. X. Ruiz, J. Giménez, I. Molist, S. Alvarez, M. Domínguez, R. Alvarez, A. R. de Lera, X. Parés, J. Farrés, Aldo-keto reductases in retinoid metabolism: search for substrate specificity and inhibitor selectivity, *Chem. Biol. Interact.* 202 (2013) 186–194.
- [10] L. Zhang, H. Zhang, Y. Zhao, Z. Li, S. Chen, J. Zhai, Y. Chen, W. Xie, Z. Wang, Q. Li, X. Zheng, X. Hu, Inhibitor selectivity between aldo-keto reductase superfamily

- members AKR1B10 and AKR1B1: role of Trp112 (Trp111). *FEBS Lett.* 587 (2013) 3681–3686.
- [11] O. El-Kabbani, A. Podjarny, Selectivity determinants of the aldose and aldehyde reductase inhibitor-binding sites, *Cell. Mol. Life Sci.* 64 (2007) 1970–1978.
- [12] T. Kinoshita, H. Miyake, T. Fujii, S. Takakura, T. Goto, The structure of human recombinant aldose reductase complexed with the potent inhibitor zenarestat, *Acta Crystallogr. Sect. D Biol. Crystallogr.* 58 (2002) 622–626.
- [13] C. Rechlin, F. Scheer, F. Terwesten, T. Wulsdorf, E. Pol, V. Fridh, P. Toth, W. E. Diederich, A. Heine, G. Klebe, Price for opening the transient specificity pocket in human aldose reductase upon ligand binding: structural, thermodynamic, kinetic, and computational analysis, *ACS Chem. Biol.* 12 (2017) 1397–1415.
- [14] J. Liu, G. Wen, D. Cao, aldo-keto reductase family 1 member B1 inhibitors: old drugs with new perspectives, *Recent Pat. Anticancer. Drug Discov.* 4 (2009) 246–253.
- [15] K. Metwally, H. Pratsinis, D. Kletsas, Pyrimido[4,5-*c*]quinolin-1(2*H*)-ones as a novel class of antimitotic agents: synthesis and *in vitro* cytotoxic activity, *Eur. J. Med. Chem.* 42 (2007) 344–350.
- [16] K. Metwally, O. Aly, E. Aly, A. Banerjee, R. Ravindra, S. Bane, Synthesis and biological activity of 2,5-diaryl-3-methylpyrimido[4,5-*c*]quinolin-1(2*H*)-one derivatives, *Bioorganic Med. Chem.* 15 (2007) 2434–2440.
- [17] K. Metwally, A. Khalil, H. Pratsinis, D. Kletsas, Synthesis, *in vitro* cytotoxicity, and a preliminary structure-activity relationship investigation of pyrimido[4,5-*c*]quinolin-1(2*H*)-ones, *Arch. Pharm. Chem. Life Sci.* 8 (2010) 465–472.
- [18] K. Metwally, A. Khalil, A. Sallam, H. Pratsinis, D. Kletsas, , K. El-Sayed, Structure-activity relationship investigation of methoxy substitution on anticancer pyrimido[4,5-*c*]quinolin-1(2*H*)-ones, *Med. Chem. Res.* 22 (2013) 4481–4491.
- [19] K. Metwally, H. Pratsinis, D. Kletsas, The antimitotic pyrimido[4,5-*c*]quinolin-1(2*H*)-one scaffold: probing substituents at position 3, *Med. Chem. Res.* 24 (2015) 2604–2611.
- [20] E. Dvornik, N. Simard-Duquesne, M. Krami, K. Sestanj, K. H. Gabbay, J. H. Kinoshita, S. D. Varma, L. O. Merola, Polyol accumulation in galactosemic and

- diabetic rats: control by an aldose reductase inhibitor, *Science* 182 (1973) 1146–1148.
- [21] S. Ao, Y. Shingu, C. Kikuchi, Y. Takano, K. Nomura, T. Fujiwara, Y. Ohkubo, Y. Notsu, I. Yamaguchi, Characterization of a novel aldose reductase inhibitor, FR74366, and its effects on diabetic cataract and neuropathy in the rat, *Metabolism* 40 (1991) 77–87.
- [22] A. S. Grewal, S. Bhardwaj, D. Pandita, V. Lather, B. S. Sekhon, Updates on aldose reductase inhibitors for management of diabetic complications and non-diabetic diseases, *Mini-Reviews Med. Chem.* 16 (2016) 120–162.
- [23] G. Maggiora, M. Vogt, D. Stumpfe, J. Bajorath, Molecular similarity in medicinal chemistry, *J. Med. Chem.* 57 (2014) 3186–3204.
- [24] T. W. H. Backman, Y. Cao, T. Girke, ChemMine tools: an online service for analyzing and clustering small molecules, *Nucleic Acids Res.* 39 (2011) 486–491.
- [25] G. A. Patani, E. J. LaVoie, Bioisosterism: a rational approach in drug design, *Chem. Rev.* 96 (1996) 3147–3176.
- [26] J. Poletto, D. W. Powell, D. H. Boschelli, Substituted quinoline carboxylic acids, U.S. patent, 4,968,702, 1990.
- [27] L. F. Raveglia, G. A. M. Giardina, M. Grugni, R. Rigolio, C. A. Farina, Novel synthesis of 3-halo-2-phenylquinoline-4-carboxylic acids, *J. Heterocycl. Chem.* 34 (1997) 557–559.
- [28] E. I. Howard, R. Sanishvili, R. E. Cachau, A. Mitschler, B. Chevrier, P. Barth, V. Lamour, M. Van Zandt, E. Sibley, C. Bon, D. Moras, T. R. Schneider, A. Joachimiak, A. Podjarny, Ultrahigh resolution drug design I: details of interactions in human aldose reductase-inhibitor complex at 0.66 Å, *Proteins Struct. Funct. Bioinforma.* 55 (2004) 792–804.
- [29] H. Steuber, A. Heine, A. Podjarny, G. Klebe, Merging the binding sites of aldose and aldehyde reductase for detection of inhibitor selectivity-determining features, *J. Mol. Biol.* 379 (2008) 991–1016.
- [30] J. Fanfrlík, F. X. Ruiz, A. Kadlčíková, J. Řezáč, A. Cousido-Siah, A. Mitschler, S. Haldar, M. Lepšík, M. H. Kolář, P. Majer, A. D. Podjarny, P. Hobza, The effect of halogen-to-hydrogen bond substitution on human aldose reductase inhibition, *ACS*

- Chem. Biol. 10 (2015) 1637–1642.
- [31] J. Fanfrlík, M. Kolář, M. Kamlar, D. Hurný, F. X. Ruiz, A. Cousido-Siah, A. Mitschler, J. Řezáč, E. Munusamy, M. Lepšík, P. Matějček, J. Veselý, A. Podjarny, P. Hobza, Modulation of aldose reductase inhibition by halogen bond tuning, *ACS Chem. Biol.* 8 (2013) 2484–2492.
- [32] D. J. Murphy, determination of accurate KI values for tight-binding enzyme inhibitors: an in Silico study of experimental error and assay design, *Anal. Biochem.* 327 (2004) 61–67.
- [33] C. Sheng, X. Che, W. Wang, S. Wang, Y. Cao, Z. Miao, J. Yao, W. Zhang, Design and synthesis of novel triazole antifungal derivatives by structure-based bioisosterism, *Eur. J. Med. Chem.* 46 (2011) 5276–5282.
- [34] M. Chatzopoulou, P. Alexiou, E. Kotsampasakou, V. J. Demopoulos, Novel aldose reductase inhibitors: a patent survey (2006 – present), *Expert Opin. Ther. Pat.* 22 (2012) 1303–1323.
- [35] O. Kraemer, I. Hazemann, A. D. Podjarny, G. Klebe, Virtual screening for inhibitors of human aldose reductase, *Proteins Struct. Funct. Bioinforma.* 55 (2004) 814–823.
- [36] Z. Otwinowski, W. Minor, Processing of X-ray diffraction data collected in oscillation mode, *Methods Enzymol.* 276 (1997) 307–326.
- [37] A. J. McCoy, R. W. Grosse-Kunstleve, P. D. Adams, M. D. Winn, L. C. Storoni, R. J. Read, Phaser crystallographic software, *J. Appl. Crystallogr.* 40 (2007) 658–674.
- [38] G. N. Murshudov, P. Skubák, A. A. Lebedev, N. S. Pannu, R. A. Steiner, R. A. Nicholls, M. D. Winn, F. Long, A. A. Vagin, REFMAC5 for the refinement of macromolecular crystal structures, *Acta Crystallogr. D. Biol. Crystallogr.* 67 (2011) 355–367.
- [39] P. D. Adams, P. V. Afonine, G. Bunkóczi, V. B. Chen, I. W. Davis, N. Echols, J. J. Headd, L.-W. Hung, G. J. Kapral, R. W. Grosse-Kunstleve, A. J. McCoy, N. W. Moriarty, R. Oeffner, R. J. Read, D. C. Richardson, J. S. Richardson, T. C. Terwilliger, P. H. Zwart, PHENIX: a comprehensive python-based system for macromolecular structure solution, *Acta Crystallogr. D. Biol. Crystallogr.* 66 (2010) 213–221.
- [40] N. W. Moriarty, R. W. Grosse-Kunstleve, P. D. Adams, Electronic ligand builder

- and optimization workbench (eLBOW): a tool for ligand coordinate and restraint generation, *Acta Crystallogr. D. Biol. Crystallogr.* 65 (2009) 1074–1080.
- [41] P. Emsley, B. Lohkamp, W. G. Scott, K. Cowtan, Features and development of Coot, *Acta Crystallogr. D. Biol. Crystallogr.* 66 (2010) 486–501.
- [42] G. M. Morris, R. Huey, W. Lindstrom, M. F. Sanner, R. K. Belew, D. S. Goodsell, A. J. Olson, AutoDock4 and AutoDockTools4: automated docking with selective receptor flexibility, *J. Comput. Chem.* 30 (2009) 2785–2791.
- [43] A. W. Schüttelkopf, D. M. F. van Aalten, PRODRG: a tool for high-throughput crystallography of protein-ligand complexes, *Acta Crystallogr. D. Biol. Crystallogr.* 60 (2004) 1355–1363.
- [44] J. De Ruyck, M. Famerée, J. Wouters, E. A. Perpète, J. Preat, D. Jacquemin, Towards the understanding of the absorption spectra of NAD(P)H/NAD(P)⁺ as a common indicator of dehydrogenase enzymatic activity, *Chem. Phys. Lett.* 450 (2007) 119–122.
- [45] F. X. Ruiz, O. Gallego, A. Ardèvol, A. Moro, M. Domínguez, S. Alvarez, R. Alvarez, A. R. de Lera, C. Rovira, I. Fita, X. Parés, J. Farrés, Aldo-keto reductases from the AKR1B subfamily: retinoid specificity and control of cellular retinoic acid levels, *Chem. Biol. Interact.* 178 (2009) 171–177.
- [46] R. J. Turner, S. J. Charlton, Assessing the minimum number of data points required for accurate IC₅₀ determination, *Assay Drug Dev. Technol.* 3 (2005) 525–531.
- [47] R.A. Copeland, Tight binding inhibitors. In *Enzymes: A Practical Introduction to Structure, Mechanism, and Data Analysis*. Wiley-VCH Inc, New York, 2000, pp. 306-317.
- [48] F. Denizot, R. Lang, Rapid colorimetric assay for cell growth and survival, *J. Immunol. Methods* 89 (1986) 271–277.
- [49] I. K. Kostakis, R. Tenta, N. Pouli, P. Marakos, A. L. Skaltsounis, H. Pratsinis, D. Kletsas, Design, synthesis, and antiproliferative activity of some novel aminosubstituted xanthenones, able to overcome multidrug resistance toward MES-SA/Dx5 cells, *Bioorganic Med. Chem. Lett.* 15 (2005) 5057–5060.

Supplementary data

Similarity Analysis

A Tanimoto similarity analysis was conducted to evaluate whether or not our compounds were potentially new chemical scaffolds compared to published ARIs. The studied compounds were compared to a database of 1,790 published ARIs extracted from the BindingDB, using as a target "Aldose reductase". The Tanimoto similarity coefficient (Tc) of this scaffold is less than or equal to 30% in pairwise comparison in both cases (22% vs. zenarestat and 30% vs. alrestatin, and less than 40% in comparison with the rest of ARIs published, Table S1. Their maximum common substructure (MCS), which allows a more accurate similarity measure for compounds with large size differences, increases to 38% and 60%, respectively. When the comparison is done replacing the 2-amino by the 2-acetic acid group, their Tc values increase to 33% and 37%, while their MCS values rise to 42% and 62%, respectively.

Table S1: Compound similarity to previously published ARIs.

Compound	Tanimoto coefficient
37	0.388
38	0.386
39	0.380
40	0.378
41	0.377
42	0.383
43	0.376
44	0.373
45	0.380
46	0.383
47	0.380
48	0.365
64	0.380
65	0.383
66	0.384
67	0.394
68	0.392
69	0.383
70	0.384

Comparison of the studied compounds to published ARIs, using the webserver Binding DB (<http://www.bindingdb.org>).

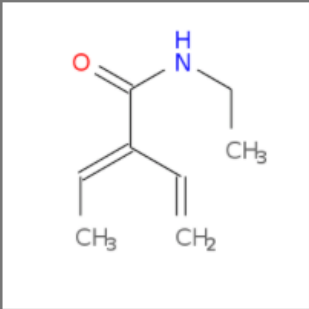
Pairwise similarity calculations were performed with <http://chemmine.ucr.edu/similarity/>. The corresponding calculations are displayed in the following pages:

-Similarity between the **2-aminopyrimido[4,5-c]quinolin-1(2H)-one** scaffold and zenarestat:

Chemmine Tools Similarity WorkBench

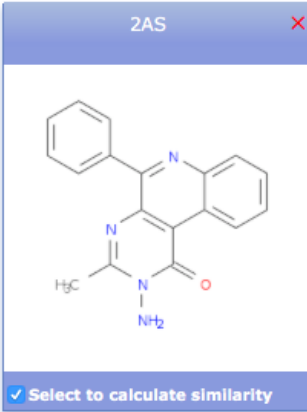
AP Tanimoto Similarity: 0.221987
 MCS Size: 10
 MCS MIN Similarity: 0.4348
 MCS MAX Similarity: 0.3846
 MCS Tanimoto Similarity: 0.2564

Loaded



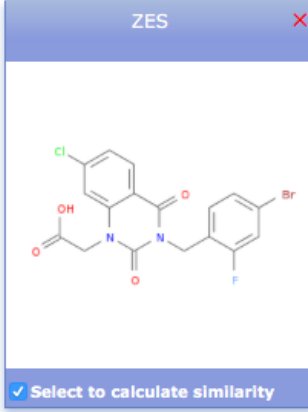
Add to Workspace

2AS



Select to calculate similarity

ZES




Select to calculate similarity

-Similarity between the **2-aminopyrimido[4,5-c]quinolin-1(2H)-one** scaffold and alrestatin:

Chemmine Tools Similarity WorkBench

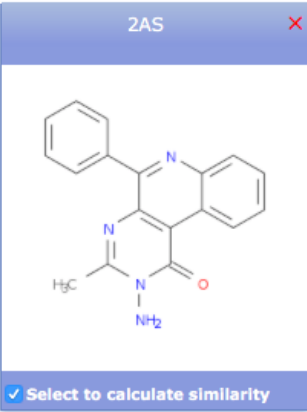
AP Tanimoto Similarity: 0.300613
 MCS Size: 14
 MCS MIN Similarity: 0.7368
 MCS MAX Similarity: 0.6087
 MCS Tanimoto Similarity: 0.5000

Loaded



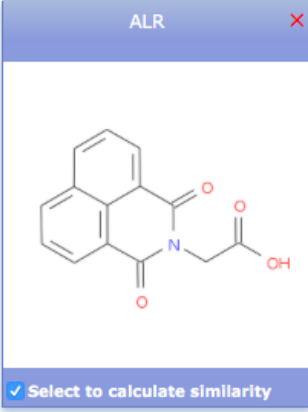
Add to Workspace

2AS



Select to calculate similarity

ALR



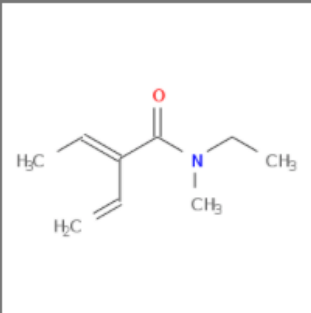
Select to calculate similarity

-Similarity between the 1-oxo-pyrimido[4,5-c]quinoline-2-acetic acid scaffold and zenarestat:

Chemmine Tools **Similarity WorkBench**

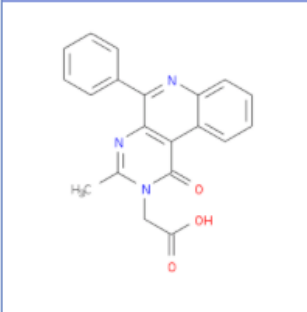
AP Tanimoto Similarity:0.337449
MCS Size:11
MCS MIN Similarity:0.4231
MCS MAX Similarity:0.4231
MCS Tanimoto Similarity:0.2683

Loaded



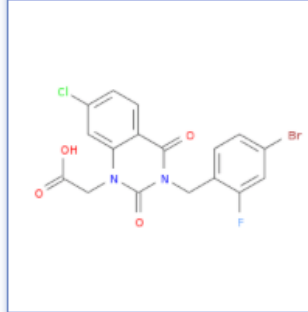
[Add to Workspace](#)

2AAS



☒ Select to calculate similarity

ZES



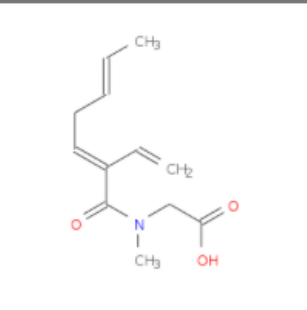
☒ Select to calculate similarity

-Similarity between the 1-oxo-pyrimido[4,5-c]quinoline-2-acetic acid scaffold and alrestatin:

Chemmine Tools **Similarity WorkBench**

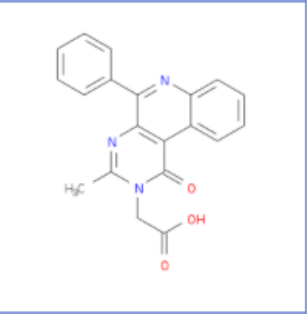
AP Tanimoto Similarity:0.373961
MCS Size:16
MCS MIN Similarity:0.8421
MCS MAX Similarity:0.6154
MCS Tanimoto Similarity:0.5517

Loaded



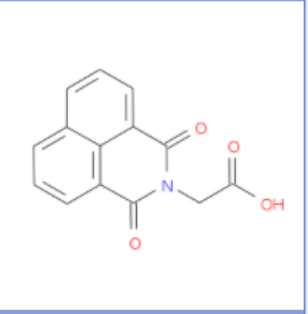
[Add to Workspace](#)

2AAS



☒ Select to calculate similarity

ALR



☒ Select to calculate similarity

Table S2. Properties calculation for the Lipinski's rule of five.

	cLogP	tPSA (Å ²)	MW	nON	nOHNH	n.viol	RB	MV (Å ³)
Acceptable range →	<5		<500	<10	<5			
Compound								
37	3.17	85.09	379.8	6	1	0	3	313.37
38	3.3	85.09	424.25	6	1	0	3	317.72
39	2.33	85.09	397.79	6	1	0	3	318.31
40	2.46	85.09	442.24	6	1	0	3	322.65
41	1.71	94.32	393.37	7	1	0	4	330.31
42	3.82	85.09	414.25	6	1	0	3	326.91
43	3.95	85.09	458.7	6	1	0	3	331.26
44	3.2	94.32	409.83	7	1	0	4	338.92
45	3.95	85.09	458.7	6	1	0	3	331.26
46	4.08	85.09	503.15	6	1	1	3	335.61
47	3.59	85.09	393.83	6	1	0	3	329.93
48	3.2	94.32	409.83	7	1	0	4	338.92
64	5.14	85.09	455.9	6	1	1	5	385.02
65	5.82	85.09	490.35	6	1	1	5	398.56
66	5.14	85.09	455.9	6	1	1	5	385.02
67	2.49	85.09	345.36	6	1	0	3	299.84
68	3.74	85.09	393.83	6	1	0	4	330.18
69	4.24	85.09	407.86	6	1	0	5	346.98
70	2.91	85.09	411.82	6	1	0	4	335.11
Commercially available AKR1B1 inhibitors								
Zenarestat	0.4	84.1	440.6	6	0	0	4	302.4
Alrestatin	-1.4	79.2	254.2	5	0	0	2	209
Epalrestat	-0.3	62.1	318.4	4	0	0	4	263.4
Zopolrestat	0.8	87.9	418.4	6	0	0	5	319.3
Tolrestat	0.9	52.6	356.3	4	0	0	6	283.1

cLogP: Calculated octanol-water partition coefficient. tPSA: Total molecular polar surface area; MW: Molecular weight; nON: Number of hydrogen bond acceptors; nOHNH: Number of hydrogen bond donors; n.viol: Number of Lipinski's rules violations; RB: Number of rotatable bonds; MV: Molecular volume. In red, violations of Lipinski's rules are highlighted. Data calculated with the website <http://www.molinspiration.com>

Table S3. Data collection and refinement statistics.

	AKR1B1-NADP⁺-37*	AKR1B1-NADP⁺-39*	AKR1B1-NADP⁺-41
PDB ID	5OU0	5OUJ	5OUK
Wavelength (Å)	0.800000	0.800000	0.800000
Resolution range (Å)	31.53 - 0.939 (0.9726 - 0.939)	28.85 - 0.96 (0.9946 - 0.96)	21.55 - 0.959 (0.9933 - 0.959)
Space group	<i>P</i> 1	<i>P</i> 1	<i>P</i> 1
Unit cell (Å)	39.76 46.77 47.16 76.45 67.76 78.18	40.05 46.98 47.28 76.40 67.57 77.40	40.29 47.08 47.30 76.34 67.52 76.76
Total reflections	599112	570950	549190
Unique reflections	181549 (14598)	173015 (14408)	171622 (13444)
Multiplicity	3.3 (2.8)	3.3 (2.7)	3.2 (2.6)
Completeness (%)	91.9 (74.7)	92.5 (77.4)	91.0 (72.5)
Mean I/sigma(I)	38.9 (4.2)	48.2 (3.4)	36.4 (4.03)
Wilson B-factor	8.14	8.91	8.22
R-mean	2.5 (23.2)	2.2 (27.0)	2.7 (23.2)
Reflections used in refinement	181521 (14591)	172979 (14395)	171598 (13437)
Reflections used for R-free	9073 (714)	8677 (729)	8558 (695)
R-work	0.1304 (0.1916)	0.1299 (0.1836)	0.1348 (0.1836)
R-free	0.1433 (0.2097)	0.1464 (0.2022)	0.1487 (0.1972)
Number of non-hydrogen atom	3210	3135	3225
macromolecules	2673	2660	2649
ligands	75	76	77
Protein residues	316	316	316
RMS (bonds)	0.017	0.018	0.018
RMS (angles)	1.87	1.56	1.52
Ramachandran favored (%)	98	99	98
Ramachandran allowed (%)	1.8	1.2	2.1
Ramachandran outliers (%)	0	0	0
Rotamer outliers (%)	0.33	0	0
Clashscore	3.65	1.46	1.65
Average B-factor	13.33	14.36	15.59
macromolecules	11.86	13.11	13.29
ligands	7.92	18.59	10.65
solvent	22.70	21.86	28.57

Statistics for the highest-resolution shell are shown in parentheses.

* Friedel mates were averaged when calculating reflection statistics.

Supplementary Figures

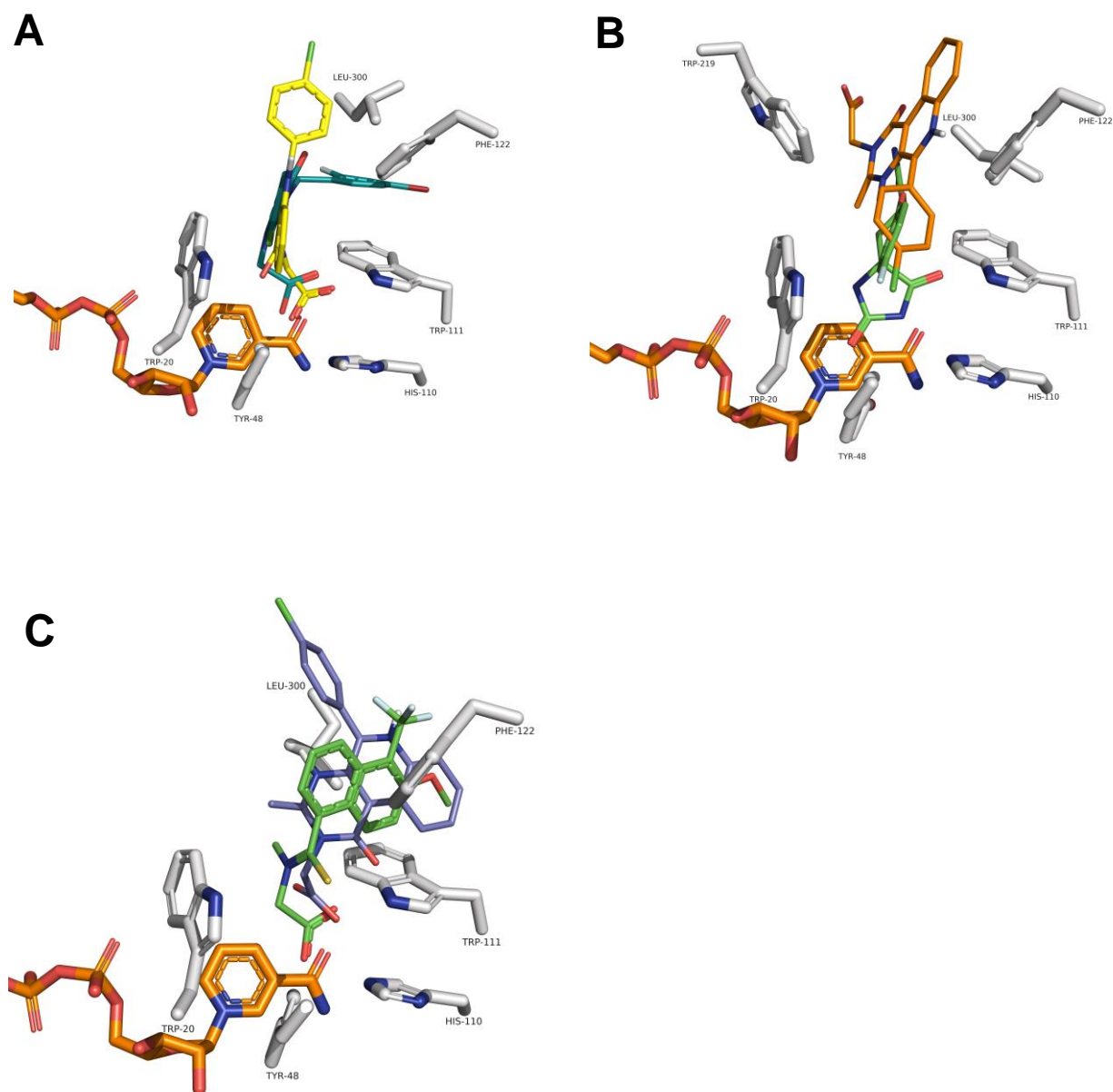


Figure S1. Computed binding mode of **2-aminopyrimido[4,5-c]quinolin-1(2H)-one** in different reference pockets. A) Zenarestat pocket (PDB 1IEI), Zenarestat is shown as green sticks and the test compound as gold sticks. B) Fidarestat pocket (PDB 1PWM), Fidarestat is shown as green sticks and the test compound as orange sticks. C) Tolrestat pocket (PDB 2FZD), Tolrestat is shown as green sticks and the test compound as blue sticks. The interacting AKR1B1 residues are displayed in white sticks and the NADP⁺ molecule in orange sticks.

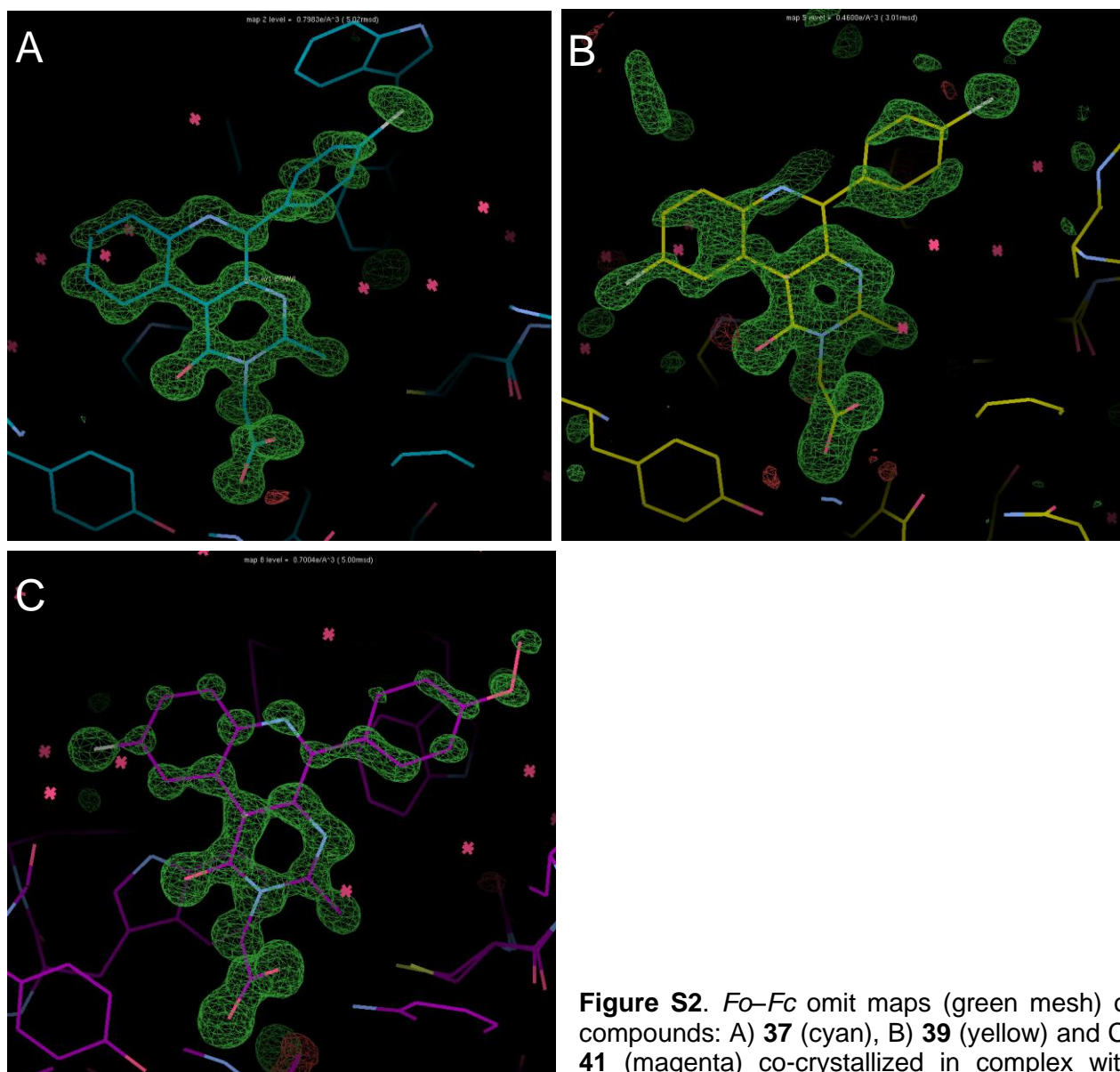


Figure S2. *Fo-Fc* omit maps (green mesh) of compounds: A) **37** (cyan), B) **39** (yellow) and C) **41** (magenta) co-crystallized in complex with AKR1B1 holoenzyme. The contoured is at 5 σ level for compounds **37** and **41**, while compound **39** is contoured at 3 σ level.

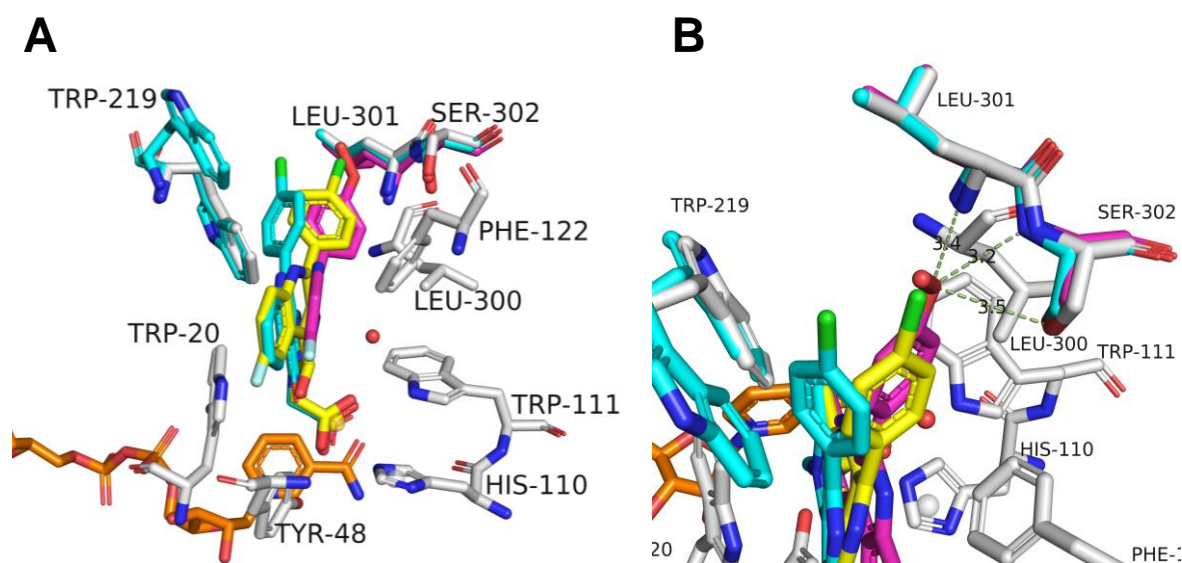


Figure S3. Superimposition of the X-ray structures of AKR1B1 holoenzyme with compounds **37** (cyan), **39** (yellow) and **41** (magenta). The cofactor is in orange sticks and the protein is in white sticks for the AKR1B1-**37** complex and in sticks coloured as the inhibitor for the other complexes. A) Overall atomic view. B) Detailed atomic view of the interaction of the 5-phenyl moiety with AKR1B1 residues Leu301 and Ser302.

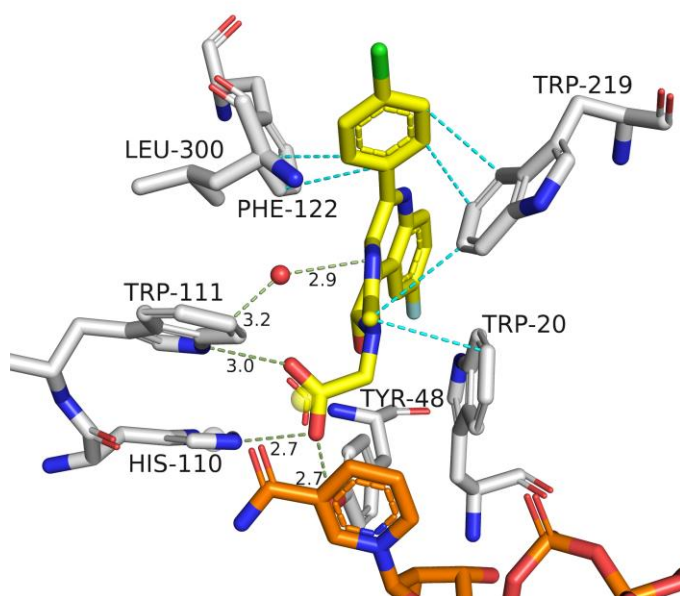


Figure S4. Back view atomic representation of the active site of AKR1B1 holoenzyme complexed with **39**. The cofactor is in orange sticks and the protein is in white sticks, with distances in Å, hydrogen bonds displayed with blue dashed lines and hydrophobic contacts in yellow dashed lines.

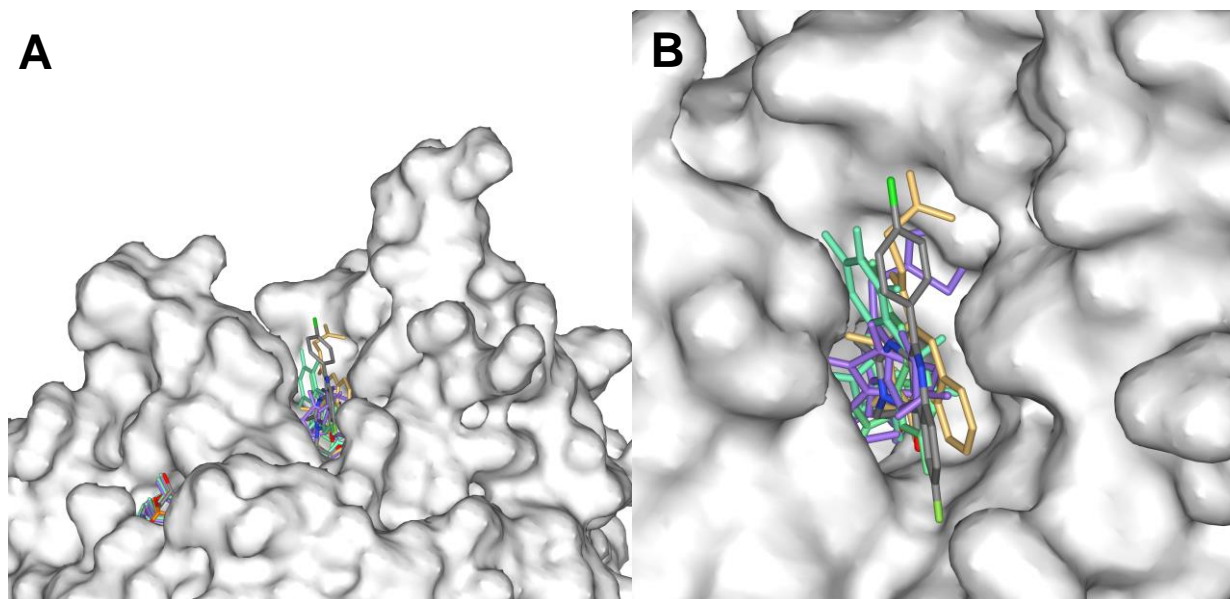


Figure S5. Superimposition of inhibitor molecules partially filling the loop B region of AKR1B1. Compound **39** in grey (PDB 5OUJ), lidorestat in violet (PDB 1Z3N), novel naphtho[1,2-*d*]isothiazole acetic acid derivative (3) in brown (PDB 2NVC), novel naphtho[1,2-*d*]isothiazole acetic acid derivative (2) in green (PDB 2NVD), and JF0064 in pale green (PDB 4IGS). A) General view. B) Close up view.